

Response to the Anonymous Referee#1's comments (acp-2016-680-RC1)

The authors have dealt with my suggestions made during preliminary review. Thank you for helping me better understand your study. I had missed that improvement of RMSE was large in my first read through. Overall the paper is well written and referenced. In regards to the choice of region, I think the discussion does a good job of making the case for South Asia being the most challenging test case for new methods.

Authors: We express our sincere thanks to the anonymous referee for his/her insightful and constructive comments and suggestions on this study. The comment/suggestions were to-the-point and very valuable for us to improve the scientific and technical clarity and quality of the manuscript. In the following, we itemize our point-by-point response to each of the concerns raised by the referee.

Comment:1 Line 133: I think there is a typo on this line.

Authors: The sentence is rewritten in the revised manuscript.

Authors change:

Line 144: *Quaas et al., (2008)* have adopted the *Loeb (2004)* approach for the estimate of planetary albedo.

Comment:2 Line 168: How much of an impact does the simplified surface albedo have? I would have thought that the calculation would have some sensitivity to whether it was looking over a forest or farmland. Maybe it averages out, but it seems like it might be enhancing the authors' calculation error. Sea surface albedo also varies a lot depending on meteorological conditions [Jin et al., 2011].

Author: In the present study, the surface albedo is used to simulate RF_{aci} using the RT model, therefore the simulated values of RF_{aci} are sensitive to the choice of the surface albedo but not the one computed using the statistical relationship between satellite based measurements. To estimate the sensitivity of the simulated RF_{aci} to surface albedo in response to the reviewer's remark, we used different plausible values of surface albedo in sensitivity simulations with radiative transfer model to assess its impact on the simulate the RF_{aci} and to compute the uncertainty statistics. These statistics are now reported in the revised manuscript and presented as supplementary material.

Authors change:

Line 330-340: In addition to above error budget, there are uncertainties involved in the RT simulated RF_{aci} due to various parameters as shown above. In this regard, the surface albedo plays a major role in the simulation of RF_{aci} . In the standard approach, we have considered a surface albedo value 0.15 for land and the predefined option for the ocean surface albedo is used for the oceanic regions in the present study. To quantify the uncertainties involved due to assumptions about the surface albedo, we have simulated RF_{aci} with different plausible surface albedo values

and computed statistics as shown in **Table S3(a) and S3(b)**. The statistics shows that the considered values of surface albedo are suitably representative of the study regions. In addition, RT simulation have their own limitations and uncertainties e.g. inherent code accuracy, overestimate in calculated RF due to plane-parallel bias, 3-D radiative transfer effect etc. It would be useful to explore these issues in the future.

Comment:3 Line 230: There might be a typo on this line discussing RMSE reduction.

Author: The sentence is revised and rewritten in the revised manuscript.

Authors change:

Line 265-266: The nonlinear fit increases the correlation by 21%-23% and reduce the RMSE by 0.007-0.011 W m⁻² compared to the multilinear approach.

Comment:4 Line 262: There is a typo in the last sentence. I have no other major suggestions relating to this paper and find it acceptable for publication pending minor revisions and grammar corrections.

Author: The sentence is rewritten in the revised manuscript.

Authors change:

Line 327-328: Limitation involved in this approach or uncertainties in the satellite retrievals contribute to the overall uncertainty, which is difficult to quantify.

Response to the Anonymous Referee#3's comments (acp-2016-680-RC2)

General Comments:

By extending the method of Quaas et al. (2008) to estimate RF_{aci} and developing and employing a new evaluation scheme for it, this work contributes a useful analysis to the field of aerosol-cloud interactions. Some additional clarification is necessary, though, in order to document how exactly this work complements Quaas et al. (2008) and what advantages it introduces. Furthermore, the manuscript requires extensive copy-editing; as written, some results are hard to understand due to typographical errors and the manuscript is hard to follow at times.

Authors: We express our sincere thanks to the referee for his/her insightful and constructive comments and suggestions on this study. The comment/suggestions were to-the-point and very valuable for us to improve the scientific and technical clarity and quality of the manuscript. In the following, we itemize our point-by-point response to each of the concerns raised by referee.

Comment:1 I strongly recommend that the authors request copy-editing services from Copernicus to improve the quality of the manuscript. In the Specific Comments section I have tried to document typographical and grammatical errors which produce confusion in interpreting the results, but overall there are many such corrections that should be made throughout the document.

Authors: The given specific comments are seriously considered and the typographical and grammatical errors are corrected throughout the document with the help of an expert to improve the quality of the manuscript. The suggested specific comments are seriously responded point-by-point in the revised manuscript.

Comment:2 The authors estimate N_d using an adiabatic liquid water cloud assumption. However, this assumption is invalid outside of stratiform clouds in the marine boundary layer, and similar estimates like Bennartz (2007) clearly indicate that this assumption is highly uncertain outside this type of regime. The authors should discuss the limitations of using N_d in their Central India (CI) region, and in seasons dominated by non-stratiform clouds (such as the monsoon one they analyze).

Authors: The limitation of the computation of N_d from satellite retrievals, and the associated uncertainty along with its contribution to the total uncertainty is discussed in the revised manuscript as suggested by the reviewer. This also takes into account new results on the retrievals of N_d from satellites.

Authors change:

Lines 137-144: A limitation of this assumption is that it applies rather well for the stratiform clouds in the marine boundary layer, but less so for convective clouds. A detailed explanation and uncertainty assessment are described in Bennartz, (2007) and Rausch et al., (2010). Recently, Bennartz and Rausch, (2017) show that the uncertainties in the CDNC climatology from 13-years of AQUA-MODIS observations are in the order of 30% in the stratocumulus regions and 60% to 80% elsewhere and its contribution to the total uncertainty for this study is discussed in the following section.

Comment:3 Several clarifications should be made regarding the non-linear fitting technique. First, it isn't clear on line 135 why α_5 should ever be set to 1; Quaas et al. (2008) does not seem to make this assumption - contrary to the assertion in lines 146-147 - and if the authors are suggesting this as an alternative formulation of equation (2), then some justification is necessary. For instance, in all except one of the nonlinear fits provided in Table S1, α_5 is an order of magnitude smaller than 1. Second, the authors should clarify what method is used to perform the non-linear fits with a citation if possible, even if it's something standard such as non-linear least squares, for the sake of reproducibility.

Authors: The assumption of α_5 set to be 1 was not clearly indicated in Quaas et al., (2008), apologies for this by the authors of our manuscript! - but a subsequent study, Ma et al., (2014) reassesses the same study by employing updated satellite products, where it is clearly indicated that for this study α_5 was set to 1. This second paper is now referenced in the present study for clarity about this point. Second, as per the reviewer's suggestion, more details about the nonlinear least square method are included in the revised manuscript.

Authors change:

Lines 175-177: In the present study, instead of considering $\alpha_5=1$ in the multiple regression, as in Quaas et al. (2008) and Ma et al., (2014), we obtained the values of all six fitting parameters using a nonlinear fitting approach (L-M algorithm) for each month and region.

Lines 163-175: For that purpose, we adopted the new statistical nonlinear least square fitting approach to obtain the six fitting parameters in Eq. (3). Nonlinear least square methods involve an iterative improvement to parameters values in order to minimize the residual sum of squares between the observed values and the predicated value of the dependent variables. We used the Levenberg-Marquardt (L-M) algorithm (Levenberg, 1944) in the nonlinear least square approach to adjust the parameter values in the iterative procedure. This algorithm combines the Gauss-Newton method and the gradient descent method. In the gradient descent method, the sum of the squared errors is reduced by updating the parameters in the steepest descent direction. In the Gauss-Newton method, the sum of the squared errors is reduced by assuming the least squares function is locally quadratic, and finding the minimum of the quadratic. The L-M algorithm acts more like a gradient descent method when the parameters are far from the optimal value and acts more like to Gauss-Newton method when the parameters are close to their optimal value. More detail of this method is given in the literature (Levenberg, 1944; Transtrum et al., 2010; Transtrum and Sethna, 2012).

Comment:4 In Section 3.2, the authors present an independent estimate of RF_{aci} for validation purposes using a radiative transfer code. The authors should include some discussion of how this approach differs from those in the literature, such as Bellouin et al. (2013), and what its limitations are given the dataset and methodology employed. Furthermore, if the use of the radiative transfer code is so readily evaluated in conjunction with satellite data, then what advantage does equation (2) offer in terms of developing constraints for RF_{aci} ?

Authors: As per the reviewer's suggestions the difference between the RT simulation of Bellouin et al., 2013 and in the present study is now explained in detail in the revised manuscript.

Following Quaas et al., (2008), Bellouin et al., (2013) performed a similar study (in terms of radiative forcing due to aerosol-cloud interactions) making use of the MACC aerosol reanalysis data and they used a radiative transfer code including a Monte-Carlo method to obtain the standard deviation for the analysis of uncertainty. However, in the present study, RF_{aci} is simulated using a radiative transfer code (SBDART) to evaluate the performance of the statistical approach used to compute the RF_{aci} . The use of a simple, analytical expression to assess the aerosol-cloud radiative forcing has the advantage of being very easily understandable, accessible and applicable.

Authors change:

Lines 190-195: Following the study by *Quaas et al., (2008)* study, *Bellouin et al., (2013)* performed a similar study with MACC reanalysis data, in which RT simulations, using a Monte - Carlo method, were carried out to obtain the standard deviation for the uncertainty analysis. However, in the present study, RF_{aci} is simulated using an RT model (SBDART) to validate the performance of both the statistical approaches used to compute the RF_{aci} using the statistical relationship between satellite measurements.

Comment:5 In equations (3-4) the authors require estimates of $d \ln N_d / d \ln \tau_a$ but do not state where these come from. If they use the regression approach of Quaas et al. (2008), then this should be indicated.

Authors: We are thankful to reviewer to point out the lack of sufficient information. The values of $d \ln N_d / d \ln \tau_a$ is obtained here are the same as Quaas et al., (2008); derived using a linear regression. This is now clarified in the revised manuscript.

Authors change:

Lines 151-154: $d \ln N_d / d \ln \tau_a$ is the sensitivity of cloud droplet number concentration (N_d) to a relative change in AOD. It is computed as the slope of the linear regression fit between the natural logarithm of N_d and AOD (*Quaas et al., 2008*). This value is calculated on a month-by-month basis and is unique to each region studied.

Comment:6 The discussion of uncertainty in the estimates of RF_{aci} in Section 4.2 does not seem to follow from the results presented earlier in the manuscript. On lines 258-259 the authors suggest that the nonlinear fitting approach reduces uncertainty by 20%-25%, but it is not clear where this estimate is coming from. The authors' analysis of the reduction in RMSE of planetary albedo compared to the radiative transfer simulations is not a measure of uncertainty, if that's what this statistic refers to. This estimate should be removed, and the authors should instead expand their error-propagation analysis to justify the estimate of -0.08 W/m^2 . For instance, in relation to the previous comment, how does uncertainty in the regional and seasonal estimates of $d \ln N_d / d \ln \tau_a$ influence the estimate of RF_{aci} ?

Authors: We are thankful to reviewer for his/her suggestion to expand the error analysis. According to reviewer's suggestion, we introduce the uncertainties involved in the present study due to different parameters considered in this study. The detailed information, including a table about the uncertainty budget is now included in the revised manuscript.

The reduction in RMSE of planetary albedo compared to RT simulations is not a measure of uncertainty in the present study. It is the reduction in RMSE of RF_{aci} due to nonlinear least square

approach compared to multilinear regression. Additionally we incorporated the mean relative difference in RF_{aci} due to both statistical approaches.

Authors change:

Lines 266-272: The relative difference between the RT-simulated and the statistically computed RF_{aci} are computed for both the statistical methods. The mean relative difference in RF_{aci} for anthropogenic fraction of AOD is 0.021 W m^{-2} in the nonlinear and 0.033 W m^{-2} in the multilinear statistical approach, whereas, for RF_{aci} of natural fraction of AOD, it is 0.032 W m^{-2} in nonlinear and 0.053 W m^{-2} in multilinear statistical approach. This suggests that the use of the nonlinear fitting approach reduces the uncertainty by 36%-39% compared to the multilinear regression.

Lines 298-309: The uncertainties due to sensitivity of N_d to a relative change in AOD ($d \ln N_d / d \ln \tau_a$) contribute most to the total uncertainty. For N_d sensitivities to changes in AOD, standard deviations are derived from minimum and maximum values obtained for each season. Following the study by *Bellouin et al., (2013)*, the standard deviations are derived from minimum and maximum values by defining 4-sigma interval, which covers the large range of sensitivities and spatio-temporal variabilities. To define the standard deviations in RF_{aci} due to variation in $d \ln N_d / d \ln \tau_a$, RF_{aci} is recomputed using those standard deviations of N_d sensitivities to changes in AOD. Table 2 shows the seasonal and regional sensitivities of $d \ln N_d / d \ln \tau_a$ along with their statistical standard deviation, which is computed from the minimum and maximum values for each season. The associated range in RF_{aci} both for anthropogenic and natural fraction of AOD is also shown in Table 2, where the standard deviation of RF_{aci} shows the variation due to change in $d \ln N_d / d \ln \tau_a$, which finally contribute to the total uncertainty.

Lines 314-324: In the present study, except for the statistical fitting method, all the variables and methodologies are same for both the statistical approach. Therefore, we used the relative difference between the RT-simulated and statistically computed RF_{aci} as an uncertainty due to the choice of the statistical fitting approach for both the statistical fitting methods. As shown in section 4.1, the mean relative differences for the nonlinear and multilinear approaches are 0.021 W m^{-2} and 0.033 W m^{-2} , respectively, in RF_{aci} for anthropogenic fraction, whereas, for the RF_{aci} of the natural fraction of AOD, these are 0.032 W m^{-2} and 0.053 W m^{-2} for nonlinear multilinear statistical approaches, respectively. Table 3 lists the uncertainty due to different parameters involved in the satellite-based estimate of RF_{aci} . We quantify the relative error as the square root of the sum of the squared relative errors for all individual contributions. This yields an influence of these relative uncertainties in the input quantities on the computed RF_{aci} of $\sim \pm 0.08 \text{ W m}^{-2}$.

Specific Comments:

Comment:1 Lines 12-15: This sentence is very awkward and partially repeats itself halfway through.

Authors: The sentence is rewritten in the revised manuscript.

Authors change:

Lines 11-14: Here we employ a new statistical approach to obtain the fitting parameters, determined using a non-linear least square statistical approach, for the relationship between planetary albedo and cloud properties and, further, the relationship between cloud properties and aerosol optical depth.

Comment:2 Lines 18-20: Sentence needs to clarify what is being compared against with the correlation and error statistics.

Authors: The sentence is rewritten as per the reviewer's suggestion.

Authors change:

Lines 14-20: In order to verify the performance, the results from both statistical approaches (previous and present) were compared to the results from radiative transfer simulations over three regions for different seasons. We find that the results of the new statistical approach agree well with the simulated results both over land and ocean. The new statistical approach increases the correlation by 21%-23% and reduce the error, compared to the previous approach.

Comment:3 Lines 37-38: Following McComiskey et al. (2009), $d \ln N_d / d \ln \tau_a$ is not computed using partial derivatives and is not calculated with LWP held constant; please remove this statement, or clarify how this relationship differs from the other ACI metrics that could be considered.

Authors: We are sorry to introduce the misleading information in the sentence and according to reviewer's suggestions, the sentence is removed in the revised manuscript.

Authors change:

Lines 34-39: Feingold et al. (2001, 2003); McComiskey et al., (2009) proposed a metric to quantify the microphysical component of the cloud albedo effect ($ACI = -d \ln N_d / d \ln \alpha$), where N_d is the cloud droplet number concentration and α in some proxy for the aerosol burden. A variety of proxies has been used to represent the cloud response to the change in aerosol, e, g., cloud optical depth (τ_c), cloud drop number concentration (N_d) and cloud droplet effective radius (r_e).

Comment:4 Line 39: Need to define r_e as "droplet effective radius"

Authors: r_e defined as "cloud droplet effective radius" in the revised manuscript.

Authors change:

Lines 37-39: A variety of proxies has been used to represent the cloud response to the change in aerosol, e, g., cloud optical depth (τ_c), cloud drop number concentration (N_d) and cloud droplet effective radius (r_e).

Comment:5 Lines 40-41: Because they are column integrals, metrics like aerosol optical depth do not necessarily represent just the particles impacting clouds - just the total ambient aerosol burden, particularly with respect to larger particles. Please rephrase accordingly.

Authors: The sentence is revised according to reviewer's suggestion in the revised manuscript.

Authors change:

Lines 39-41: Similarly, various proxies have been used to represent the total ambient aerosol burden, including aerosol number concentration (N_a), aerosol optical depth (τ_a) and aerosol index (AI).

Comment:6 Lines 68-74: The first sentence is something of a non-sequitur and could be removed entirely. The second sentence is awkwardly phrased; it would be better to point out that the aerosol mixture in this region is very heterogeneous in time and space with respect to size distribution and chemical composition.

Authors: The suggested sentence is removed and others are rewritten in the revised manuscript.

Authors change:

Lines 68-76: The rapid socio-economic development in the recent past has increased the anthropogenic emissions in the South Asian region along with several parts of the world. The South Asian ones are among the potential sources of a variety of aerosol species; both natural and anthropogenic, and extensive investigations are being made in the past years (e.g., *Chin et al., 2000; Di Girolamo et al., 2004; Moorthy et al., 2013*). These densely populated regions with the increasing power demand, fuel consumption and equally diverse geographical features are also vulnerable to the impacts of atmospheric aerosols to the climate (e.g. *Liu et al., 2009*).

Comment:7 Lines 82-85: It would be extremely helpful to the reader if you included a figure that outlined where these regions are on a map.

Authors: As per the reviewer's suggestions, a figure is included in the revised manuscript, which shows the study regions on a map.

Authors change:

Lines 86-91 and Figure-1 : Therefore, we discuss the RF_{aci} for both anthropogenic and natural fraction of aerosol for a period of six-years (2008-2013) for three different regions of south Asia (**Fig. 1**, Arabian Sea (AS; 63°E-72°E, 7°N-19°N), Bay of Bengal (BOB; 85°E-94°E, 7°N-19°N) and Central India (CI; 75°E-84°E, 20°N-30°N)), having significantly distinct aerosol environments as a result of variations in aerosol sources and transport pathways (*Cherian et al., 2013; Das et al., 2015; Tiwari et al., 2015*).

Comment:8 Lines 91-93: This sentence should be flipped with the following and the beginning of the paragraph re-written to emphasize that your data comes predominantly from MODIS and CERES; then you should dive into the details of which data product (and citation) you use for each specific derived quantity.

Authors: The sentence is revised as per reviewer's suggestions.

Authors change:

Lines 95-103: Data acquired by MODerate Resolution Imaging Spectroradiometer (MODIS) and Clouds and the Earth's Radiant Energy System (CERES) mounted on Aqua (*Parkinson, 2003*) and Ozone Monitoring Instrument (OMI) onboard Aura (*Schoeberl et al., 2006*) are used in this study. We use the broadband shortwave planetary albedo (α) (*Wielicki et al., 1996; Loeb, 2004; Loeb et al., 2007*) as retrieved by the CERES in combination with cloud properties from the MODIS (*Minnis et al., 2003*) and AOD (τ_a) and fine mode fraction (FMF) as retrieved by the MODIS onboard Aqua (*Remer et al., 2005*).

Comment:9 Lines 128-131: Pursuant to the general comment about N_d , the authors should discuss the limitations of this method for estimating N_d .

Authors: The limitation of N_d along with its contribution to the total uncertainty is discussed in the revised manuscript as per suggestion.

Authors change:

Lines 137-143: A limitation of this assumption is that it applies rather well for the stratiform clouds in the marine boundary layer, but less so for convective clouds. A detailed explanation and uncertainty assessment are described in *Bennartz, (2007) and Rausch et al., (2010)*. Recently, *Bennartz and Rausch, (2017)* show that the uncertainties in the CDNC climatology from 13-years of AQUA-MODIS observations are in the order of 30% in the stratocumulus regions and 60% to 80% elsewhere and its contribution to the total uncertainty for this study is discussed in the following section.

Comment:10 Line 132: Where does this particular value for γ come from?

Authors: The reference for the value of γ is added in the revised manuscript.

Authors change:

Line 137: Where, a constant value of $\gamma=1.37\times 10^{-5} \text{ m}^{-0.5}$ (*Quaas et al., 2006*) is used in this study.

Comment:11 Lines 144-152: At a minimum, this paragraph needs additional detail on what nonlinear fitting approach was used (non-linear least squares? some other method?) with a citation if applicable.

Authors: As per reviewer's suggestion, the detail about nonlinear method is discussed in the revised manuscript.

Authors change:

Lines 162-175: For that purpose, we adopted the new statistical nonlinear least square fitting approach to obtain the six fitting parameters in Eq. (3). Nonlinear least square methods involve an iterative improvement to parameters values in order to minimize the residual sum of squares between the observed values and the predicated value of the dependent variables. We used the Levenberg-Marquardt (L-M) algorithm (*Levenberg, 1944*) in the nonlinear least square approach to adjust the parameter values in the iterative procedure. This algorithm combines the Gauss-Newton method and the gradient descent method. In the gradient descent method, the sum of the squared errors is reduced by updating the parameters in the steepest descent direction. In the Gauss-Newton method, the sum of the squared errors is reduced by assuming the least squares function is locally quadratic, and finding the minimum of the quadratic. The L-M algorithm acts more like a gradient descent method when the parameters are far from the optimal value and acts more like to Gauss-Newton method when the parameters are close to their optimal value. More detail of this method is given in the literature (*Levenberg, 1944; Transtrum et al., 2010; Transtrum and Sethna, 2012*).

Comment:12 Line 164: Before this sentence, it would be useful if the authors list the variables required to perform their SBDART computations.

Authors: Following this suggestion, a list of input variables and their sources are tabulated as table-1 in the revised manuscript.

Authors change:

Lines 200-201: Table 1 shows the list of input parameters and their source provided to the RT model for the estimate of RF_{aci} .

Comment:13 Line 184-185: Please clarify the difference between τ_a and $\tau_a^{ant/nat}$. Presumably the first is the total AOD and the second is just the anthropogenic/natural contribution to AOD?

Authors: Yes, it is correct. The difference between both the terms τ_a and $\tau_a^{ant/nat}$ are clarified in the revised manuscript.

Authors change:

Lines 154-155: τ_a is the total AOD, whereas, $\tau_a^{ant/nat}$ are the anthropogenic and natural AOD, respectively, derived from the FMF and UV-AI as estimated above.

Comment:14 Line 185 and Equation 5: I would recommend writing out explicitly $N'_d = N_d + \Delta N_d$ in both locations.

Authors: Terms are modified as per reviewer's suggestions.

Authors change:

Lines 220-221: The perturbed value of N'_d ($N_d + \Delta N_d$) is used to obtain a perturbed value of r_e using Eq. (5) for constant liquid water content because r_e is used as an input to the radiative transfer code.

Equation -5

$$N'_d = q_l / \left(\frac{4}{3} \pi r_e^3 \rho_w \right) \quad (1)$$

Comment:15 Lines 202-203: “Weight” is the wrong word; according to Table S1, it's simply that the magnitude of the coefficients are different.

Authors: The word “weight” is replaced by “magnitude of the coefficient” as per reviewer's suggestion.

Authors change:

Lines 237-239: The magnitude of the coefficients α_4 and α_6 is larger in the nonlinear fit than the multilinear regression fitting, which may reduce the magnitude of the coefficient α_5 .

Comment:16 Lines 225-227: Rephrase to avoid using terms like “satisfactory results” in preference for neutral language.

Authors: The term “satisfactory results” is replaced in the revised manuscript.

Authors change:

Lines 260-261: The analysis showed good statistical agreement with Pearson's correlation coefficient $r=0.82$ and 0.75 and $RMSE=0.037 \text{ Wm}^{-2}$ and 0.042 Wm^{-2} for the anthropogenic and natural fraction of aerosols, respectively.

Comment:17 Lines 229-231: The phrasing “. . . decreases RMSE by from 0.007 to 0.011 . . .” is clearly a mistake; please delete whichever word is wrong and be clear about how the RMSE is changing.

Authors: The sentence is revised and rewritten in the revised manuscript.

Authors change:

Lines 264-272: The nonlinear fit increases the correlation by 21%-23% and reduce the RMSE by 0.007-0.011 W m⁻² compared to the multilinear approach. The relative difference between the RT-simulated and the statistically computed RF_{aci} are computed for both the statistical methods. The mean relative difference in RF_{aci} for anthropogenic fraction of AOD is 0.021 W m⁻² in the nonlinear and 0.033 W m⁻² in the multilinear statistical approach, whereas, for RF_{aci} of natural fraction of AOD, it is 0.032 W m⁻² in nonlinear and 0.053 W m⁻² in multilinear statistical approach. This suggests that the use of the nonlinear fitting approach reduces the uncertainty by 36%-39% compared to the multilinear regression.

A new statistical approach to improve the satellite based estimation of the radiative forcing by aerosol- cloud interactions

Piyushkumar N Patel¹, Johannes Quaas², Raj Kumar¹

¹Space Applications Centre, ISRO, Ahmedabad, India

²Institute for Meteorology, Universität Leipzig, Leipzig, Germany

Corresponding to: Piyushkumar N Patel (piyushether@gmail.com)

Abstract

In a previous, study of *Quaas et al., (2008)* the radiative forcing by anthropogenic aerosol due to aerosol-cloud interactions, RF_{aci} , was obtained by a statistical analysis of satellite retrievals using a multilinear regression. Here we employ a new statistical approach to obtain the ~~six~~ fitting parameters, determined using a non-linear least square statistical approach ~~to obtain the six fitting parameters~~, for the relationship between planetary albedo and cloud properties and, further, the relationship ~~of the between~~ cloud properties and aerosol optical depth. ~~The statistical approach is~~ In order to verify the performance, the results from both statistical approaches (previous and present) were compared to the results from radiative transfer simulations over three ~~different~~ regions ~~and~~ for different seasons. We find that the results of the new statistical approach agree well with the simulated results both over ~~both~~ land and ocean. The new statistical approach increases the correlation ~~coefficient of the fitted to the satellite retrieved albedo~~ by 21%-23% and ~~decreases~~reduce the error, compared to the previous approach.

1 Introduction

Aerosols are considered to have a large effect on climate, both through aerosol radiation interactions, and through aerosol-cloud interactions by serving as cloud condensation nuclei (CCN), therefore increasing N_d and thus cloud albedo (*Twomey, 1974*), as well as rapid cloud adjustments (*Boucher et al., 2013*). Much work has been done to quantify the radiative forcing by aerosol-cloud interaction (RF_{aci}), yet it remains highly uncertain. The annual radiative forcing from aerosol induced changes in cloud albedo were reported as -0.7 Wm^{-2} with an uncertainty range -1.8 to -0.3 Wm^{-2} (*Boucher et al., 2013*); this effect could offset much of the warming from greenhouse gases (*Huber and Knutti, 2011*), emphasizing the need to understand the effect so that we can better predict the future climate.

In this study, we concentrate on the RF_{aci} , the change in cloud albedo with increasing aerosol. An increasing aerosol at constant cloud water content is supposed to decrease droplet size, which in turn increases the cloud albedo due to the increase scattering of the smaller, more numerous cloud droplets. *Feingold et al. (2001, 2003); McComiskey et al., (2009)* proposed a metric to quantify the microphysical component of the cloud albedo effect ($ACI = -d \ln N_d / d \ln \alpha$), where N_d is the cloud droplet number concentration and α in some proxy for the aerosol burden. ~~Note that the partial derivatives must be calculated at constant liquid water path (LWP).~~ A variety of proxies has been used to represent the cloud response to the change in aerosol, e, g., cloud optical depth (τ_c), cloud drop number concentration (N_d) and cloud droplet effective radius (r_{e-}). Similarly, various proxies have been used to represent the total ambient aerosol ~~partieles affecting the cloud burden~~, including aerosol number concentration (N_a), aerosol optical depth (τ_a) and aerosol index (AI). An overview about published relationships and their biases due to mismatches between process- and analysis scales are

43 discussed in *McComiskey and Feingold, (2012)*. Values for ACI metrics from observations often differ
44 significantly from model-based values (*Quaas et al., 2008, 2009; Bellouin et al., 2008; Penner et al.,*
45 *2011, 2012*). For example, the observational-based values of RF_{aci} , often in the range of -0.2 to -0.6
46 Wm^{-2} (*Quaas et al., 2008; Bellouin et al., 2013*), is tend to be weaker than the modeled values in the
47 range of -0.5 to -1.9 Wm^{-2} (*IPCC, 2007*). The differences in model and observational-based RF_{aci} have
48 to be reconciled. *Penner et al., (2011)* reported that the lower sensitivities of cloud droplet number
49 concentration, when considering aerosol optical depth (AOD) compared to aerosol index as aerosol
50 quantity may lead to a significant underestimation in satellite-based RF_{aci} . However, *Quaas et al.,*
51 *(2011)* pointed out the weaknesses in the approach used by *Penner et al., (2011)*.

52 Clearly, further study is needed to reduce the uncertainties in both observational- and model-based
53 estimates of aerosol RF_{aci} and to reconcile the differences.

54 *Quaas et al., (2008)* derived the anthropogenic aerosol RF_{aci} based on satellite retrievals of aerosol
55 and clouds properties using statistical relationships between cloud properties and anthropogenic
56 aerosols without the use of radiative transfer model. They developed a statistical relationship between
57 planetary albedo and cloud properties using a multilinear fit, and further, the relationships of cloud
58 properties and aerosol optical depth. *Quaas et al. (2008)* suggested that uncertainties in the statistical
59 relationship and fitting parameters introduced uncertainty in the estimate of RF_{aci} . Therefore, it is
60 useful to reassess the estimated RF_{aci} by using a new statistical fitting approach. The main objective of
61 this study is to explore the uncertainty in the satellite-based quantification of RF_{aci} . This study differs
62 from previous studies by introducing new statistical fitting approach to obtain the fitting parameters
63 for the estimates of RF_{aci} , determined using a nonlinear fit between planetary albedo and cloud
64 properties. To verify the present approach, the results from both statistical approaches are compared
65 with the results from a radiative transfer model.

66 ~~Recent studies suggest that~~The rapid socio-economic development in the south Asian recent past
67 ~~has increased the anthropogenic emissions in the South asian region is one of the world's most~~
68 ~~populous (~24% along with several parts of the world population) region with growing industrial. The~~
69 ~~South Asian ones are among the potential sources of a variety of aerosol species; both natural and~~
70 ~~transport sectors. A large anthropogenic, and extensive investigations are being made in the past years~~
71 ~~(e.g., Chin et al., 2000; Di Girolamo et al., 2004; Moorthy et al., 2013). These densely populated~~
72 ~~regions with the~~ increasing power demand, fuel consumption, and equally diverse geographical
73 features ~~make this region among~~are also vulnerable to the ~~global hotspots~~impacts of atmospheric
74 aerosols- ~~to the climate (e.g. Liu et al., 2009)~~. The complex geography of this region contributes
75 significant amounts of natural aerosols (desert dust, pollen, sea-salt etc) into the atmosphere, which
76 mix with anthropogenic ones, making the aerosol environment one of the most complex in the world
77 (*Moorthy et al., 2015*). The large spatial heterogeneity of the sources coupled with the atmospheric
78 dynamics driven by topography and contrasting monsoons, make South Asia's aerosol very difficult
79 to characterize and to model their implications on radiative and climate forcing. While tropospheric
80 perturbations would produce strong regional signatures, their global impacts still remain marginally
81 above the uncertainty levels (*IPCC, 2013*). In the recent years, several studies are carried out on the
82 aerosol characterization and its direct effect over south Asia, but there have been very few studies
83 reported on the aerosol indirect effect using ground- and satellite-based measurements due to complex
84 aerosol and cloud environments. Therefore, we discuss the RF_{aci} for both anthropogenic and natural
85 fraction of aerosol for a period of six-years (2008-2013) for three different regions of south Asia (**Fig.**
86 **1**, Arabian Sea (AS; 63°E-72°E, 7°N-19°N), Bay of Bengal (BOB; 85°E-94°E, 7°N-19°N) and Central
87 India (CI; 75°E-84°E, 20°N-30°N)), having significantly distinct aerosol environments as a result of

88 variations in aerosol sources and transport pathways (*Cherian et al., 2013; Das et al., 2015; Tiwari et*
89 *al., 2015*) Additionally, we also discuss the uncertainties of the results in the following sections.

90 2 Data

91 We combine measurements of aerosol, cloud and radiative properties to derive the top-of-the
92 atmosphere (TOA) RF_{aci} ~~off~~ for both anthropogenic and natural aerosols. Data acquired by
93 ~~sensors~~ MODerate Resolution Imaging Spectroradiometer (MODIS) and Clouds and the Earth's
94 Radiant Energy System (CERES) mounted on Aqua (*Parkinson, 2003*) and Ozone Monitoring
95 Instrument (OMI) onboard Aura (*Schoeberl et al., 2006*) are used in this study. We use the broadband
96 shortwave planetary albedo (α) (*Wielicki et al., 1996; Loeb, 2004; Loeb et al., 2007*) as retrieved by
97 the ~~Clouds and the Earth's Radiant Energy System (CERES)~~ in combination with cloud properties
98 from the ~~MODerate Resolution Imaging Spectroradiometer (MODIS; (Minnis et al., 2003)~~ and AOD
99 (τ_a) and fine mode fraction (FMF) as retrieved by the MODIS onboard Aqua (*Remer et al., 2005*).
100 Albedo and cloud properties are from the CERES Single-Scanner-Footprint (SSF) Level-2 Edition-3A
101 data set at $20 \times 20 \text{ km}^2$ horizontal resolution and aerosol properties (AOD and FMF) at 550nm from the
102 MYD04 level-2 collection-5.1 dataset at $10 \times 10 \text{ km}^2$ horizontal resolution are used. We used UV-
103 aerosol index (UV-AI; *Torres et al., 1998*) measured by ~~Ozone Monitoring Instrument (OMI; AURA~~
104 ~~(Levelt et al., 2006) onboard Aura~~ from the OMAERUVG level-2 version 003 dataset at $0.25^\circ \times 0.25^\circ$
105 grid, which is a gridded dataset containing retrievals from the OMAERUV (*Torres et al., 2007*)
106 algorithm. The data from CERES and MODIS level-2 products are interpolated to a $0.25^\circ \times 0.25^\circ$
107 regular longitude-latitude grid to separate the aerosol and cloud properties for anthropogenic and
108 natural aerosols using UV-AI. Daily data, taken at roughly 13:30 local time, cover the 2008-2013
109 period.

110 3 Methods

111 All statistics between aerosol and cloud properties are computed separately for 3 regions and for
112 each month of data at $0.25^\circ \times 0.25^\circ$ grid resolution. To avoid the greater uncertainty that exists in a clear
113 distinction between aerosols and clouds and accurate retrieval of cloud properties, only single-layer
114 cloud with liquid water path (LWP) $> 20 \text{ gm}^{-2}$ are taken into account. RF_{aci} for anthropogenic and
115 natural aerosols are calculated using the methods outlined by *Quaas et al., (2008)* with the new
116 statistical approach. As a part of this process, the method by *Kim et al., (2007)* MODIS-OMI algorithm
117 (MOA) is employed to classify the aerosol types into one of four types sea-salt, carbonaceous, dust
118 and sulfate using MODIS FMF and OMI UV-AI data. FMF provides information on the representative
119 size of the aerosol. FMF is close to 1 for mostly small aerosol particles, which implies an anthropogenic
120 origin and FMF becomes small for non-anthropogenic aerosol like dust. UV-AI allows to detect the
121 absorption due to the presence of an aerosol layer by utilizing the sensitivity of absorptive aerosol in
122 UV. Under most condition, UV-AI is positive for absorbing aerosols and negative for non-absorbing
123 aerosols. Using these two independent data sets, aerosol can be classified. Details for the aerosol
124 classification are discussed in *Kim et al., (2007)*. For the purpose of this research, the combination of
125 dust and sea-salt AOD considered as a natural AOD and an anthropogenic AOD contains the
126 combination of carbonaceous and sulfate. Further, the RF_{aci} is estimated for both anthropogenic and
127 natural aerosols.

128 3.1 Satellite-based estimate of RF_{aci}

129 RF_{aci} is a function of the relationship between AOD and N_d in a cloud. N_d is not directly provided
130 by satellite product and must be computed using cloud optical thickness (τ_c) and effective droplet

radius (r_e) for liquid water clouds assuming adiabaticity (*Brenguier et al., 2000*); *Schüller et al., 2005*; *Quaas et al., 2006*; *Bennartz, 2007*; *Rausch et al., 2010*).

$$N_d = \gamma \tau_c^{1/2} r_e^{-5/2} \quad (2)$$

Where, $\gamma=1.37 \times 10^{-5} \text{ m}^{-0.5}$ in this study.

Where, a constant value of $\gamma=1.37 \times 10^{-5} \text{ m}^{-0.5}$ (*Quaas et al., 2006*) is used in this study. A limitation of this assumption is that it applies rather well for the stratiform clouds in the marine boundary layer, but less so for convective clouds. A detailed explanation and uncertainty assessment are described in *Bennartz, (2007)* and *Rausch et al., (2010)*. Recently, *Bennartz and Rausch, (2017)* show that the uncertainties in the CDNC climatology from 13-years of AQUA-MODIS observations are in the order of 30% in the stratocumulus regions and 60% to 80% elsewhere and its contribution to the total uncertainty for this study is discussed in the following section.

Quaas et al., (2008) have adopted the *Loeb (2004)* approach for the estimate of planetary albedo. Albedo (α) of a cloud scene can be well described by a sigmoidal fit as

$$\alpha \approx (1 - f)[a_1 + a_2 \ln \tau_a] + f[a_3 + a_4 (f \tau_c)^{a_5}]^{a_6} \quad (3)$$

Where, a_1 - a_6 are fitting parameters obtained by a multilinear regression, where a_5 is set as 1- (*Ma et al., 2014*). Dependency of τ_a is introduced to include the clear part of the scene in the above equation and f is the cloud fraction. The satellite-based estimate of RF_{aci} for anthropogenic and natural aerosols can be expressed as

$$\Delta F_{ant/nat}^{RF_{aci}} = f_{liq} A(f, \tau_c) \frac{1}{3} \frac{d \ln N_d}{d \ln \tau_a} [\ln \tau_a - \ln(\tau_a - \tau_a^{ant/nat})] S \quad (4)$$

$$\text{where, } A(f, \tau_c) = a_4 a_5 a_6 [a_3 + a_4 (f \tau_c)^{a_5}]^{a_6 - 1} (f \tau_c)^{a_5}$$

$d \ln N_d / d \ln \tau_a$ is the sensitivity of cloud droplet number concentration (N_d) to a relative change in AOD. It is computed as the slope of the linear regression fit between the natural logarithm of N_d and AOD (*Quaas et al., 2008*). This value is calculated on a month-by-month basis and is unique to each region studied. τ_a is the total AOD, whereas, $\tau_a^{ant/nat}$ are the anthropogenic and natural AOD, respectively, derived from the FMF and UV-AI as estimated above. $A(f, \tau_c)$ is the empirical function relating albedo to f and τ_c . S is the daily mean solar incoming solar radiation. RF_{aci} is calculated separately for the anthropogenic and natural aerosols for all three regions for each month. ~~$A(f, \tau_c)$ is the empirical function relating albedo to f and τ_c . $\tau_a^{ant/nat}$ is aerosol optical depth for anthropogenic and natural aerosol, respectively, S is the daily mean solar incoming solar radiation.~~

A goal of the present study is to assess the uncertainty in the satellite-based estimate of the RF_{aci} . For that purpose, we adopted the new statistical nonlinear least square fitting approach to obtain the six fitting parameters in Eq. (3). ~~Instead~~ Nonlinear least square methods involve an iterative improvement to parameters values in order to minimize the residual sum of squares between the observed values and the predicated value of the dependent variables. We used the Levenberg-Marquardt (L-M) algorithm (*Levenberg, 1944*) in the nonlinear least square approach to adjust the parameter values in the iterative procedure. This algorithm combines the Gauss-Newton method and the gradient descent method. In the gradient descent method, the sum of the squared errors is reduced by updating the parameters in the steepest descent direction. In the Gauss -Newton method, the sum of the squared errors is reduced by assuming the least squares function is locally quadratic, and finding the minimum of the quadratic. The L-M algorithm acts more like a gradient descent method when the parameters are far from the optimal value and acts more like to Gauss-Newton method when the

169 parameters are close to their optimal value. More detail of this method is given in the literature
170 ([Levenberg, 1944](#); [Transtrum et al., 2010](#); [Transtrum and Sethna, 2012](#)). In the present study, instead
171 of considering $\alpha_5=1$ in the multiple regression, as in [Quaas et al. \(2008\)](#) and [Ma et al., \(2014\)](#), we
172 obtained the values of all six fitting parameters using a nonlinear fitting approach ([L-M algorithm](#)) for
173 each month and region. To get an impression of the performance of our statistical approach, we
174 correlate α and RF_{aci} at TOA obtained from both statistical fitting methods (multilinear and nonlinear)
175 vs. α and RF_{aci} simulated by radiative transfer model for all three regions. The following section
176 describes the detail information about the simulation of α and RF_{aci} using the radiative transfer model.

177 3.2 Simulation of planetary albedo (α) and RF_{aci}

178 In order to verify both the statistical approaches, we performed a radiative transfer simulation to
179 obtain α and RF_{aci} for all three regions. Radiative transfer calculations are performed with the SBDART
180 [Santa Barbara DISORT Atmospheric Radiative Transfer; [Ricchiazzi et al., 1998](#)] that is a plane-
181 parallel radiative transfer code based on the DISORT algorithm for discrete-ordinate-method radiative
182 transfer in multiple scattering and emitting layered media ([Stamnes et al., 1988](#)). The discrete ordinate
183 method provides a numerically stable algorithm to solve the equations of plane-parallel radiative
184 transfer in a vertically inhomogeneous atmosphere. Simulations are carried out for the solar spectrum
185 (0.2-4.0 μ m) for all three regions. [Following the study by Quaas et al., \(2008\) study, Bellouin et al.,](#)
186 [\(2013\) performed a similar study with MACC reanalysis data, in which RT simulations, using a Monte](#)
187 [-Carlo method, were carried out to obtain the standard deviation for the uncertainty analysis. However,](#)
188 [in the present study, \$RF_{aci}\$ is simulated using an RT model \(SBDART\) to validate the performance of](#)
189 [both the statistical approaches used to compute the \$RF_{aci}\$ using the statistical relationship between](#)
190 [satellite measurements.](#)

191 In the present study, simulations are carried out to simulate first α and later RF_{aci} for the given
192 inputs. Here α is evaluated as the ratio of broadband outgoing (or upwelling) shortwave flux to the
193 incoming (or downwelling) solar flux. Inputs to the model include profiles of temperature and water
194 vapor which are resolved into 32 layers extending from 1000 to 1 mbar and come from European
195 Centre for Medium-range Weather Forecast (ECMWF) reanalysis data. [Table 1 shows the list of input](#)
196 [parameters and their source provided to the RT model for the estimate of \$RF_{aci}\$.](#) Total columnar amount
197 of atmospheric ozone is provided from OMI-AURA. Surface albedo is set to 0.15 to represent a typical
198 land cover value for CI and, predefined option of the ocean surface is used for the oceanic regions (AS
199 and BOB). In the SBDART model, the cloud parameter inputs are effective droplet radius (r_e), liquid
200 water path (LWP) and the cloud fraction, all of which are taken from MODIS retrievals reported in the
201 CERES-SSF product. The geometrical thickness of cloud (CGT) is computed as a difference between
202 cloud top and bottom heights. Cloud top height is taken from CERES-SSF product and cloud base
203 height is evaluated using the geopotential height profile from ECMWF data. Only liquid water clouds
204 are considered in the estimation of RF_{aci} . The upwelling and downwelling fluxes are computed
205 individually computed for all three regions at satellite (MODIS-Aqua as a reference) overpass time.

206 The local radiative forcing associated with the RF_{aci} is estimated as the difference between the
207 perturbed and unperturbed radiative fluxes caused by perturbation in N_d due to the addition of aerosols
208 while keeping the same meteorology. RF_{aci} is diagnosed by making two calls to the radiative transfer
209 code: the first call used the unperturbed satellite-derived N_d and the second used perturbed N_d due to
210 anthropogenic and natural aerosols. The numerical evaluation of radiative flux for the perturbed case
211 starts by determining the finite perturbation of cloud droplet number concentration (ΔN_d), calculated
212 as follows:

$$\Delta N_d^{ant/nat} = \frac{d \ln N_d}{d \ln \tau_a} [\ln \tau_a - \ln(\tau_a - \tau_a^{ant/nat})] \quad (5)$$

213 The finite perturbation in N_d are evaluated separately for anthropogenic and natural aerosol to estimate
 214 the radiative flux for the perturbed case. The perturbed value of $\dot{N}_d N'_d$ ($N_d + \Delta N_d$) is used to obtain a
 215 perturbed value of r_e using Eq. (5) for constant liquid water content because r_e is used as an input to
 216 the radiative transfer code.

$$\dot{N}_d = q_l / \left(\frac{4}{3} N'_d\right) = q_l / \left(\frac{4}{3} \pi r_e^3 \rho_w\right) \quad (6)$$

217 Where, ρ_w is the liquid water density, q_l the liquid water content (q_l =liquid water path / geometrical
 218 thickness). RF_{aci} is diagnosed as $RF_{unperturbed} - RF_{perturbed}$ radiative fluxes at the top of the atmosphere,
 219 because increased concentrations of aerosol reduce the effective radius of cloud particles and smaller
 220 cloud particles reflect more radiation back to space. The following section describes the details of
 221 regression analysis of α and RF_{aci} performed between values from statistical-approaches and simulated
 222 values.

223 4 Results

224 4.1 Regression analysis

225 As stated in section 3.1, the satellite-based estimates of RF_{aci} are dependent on the fitting parameters
 226 α_1 - α_6 , obtained here from the two different statistical fitting approaches (multilinear and nonlinear).
 227 The parameters obtained from these two approaches are listed in [Table_S1](#) for all three regions
 228 investigated in this study. These parameters vary with months since we conducted both the fitting
 229 approaches for each month, but only the mean seasonal parameters are shown here. The main
 230 differences in fitting parameters from both methods are found in the values of α_4 , α_5 and α_6 . The ~~weight~~
 231 ~~given to magnitude of the coefficients~~ α_4 and α_6 ~~is larger~~ in the nonlinear fit ~~is larger than for~~
 232 the multilinear regression fitting, which may reduce the ~~weight~~ ~~magnitude~~ of the ~~coefficient~~ α_5 .

233 To accomplish the objective of this study, we correlate α and RF_{aci} at TOA obtained from both
 234 statistical fitting approaches (multilinear and nonlinear) with estimates obtained from radiative transfer
 235 model for all three regions. [Fig. 12](#) shows scatter density plots of comparison between model-simulated
 236 albedo and the one computed from satellite measurements at $0.25^\circ \times 0.25^\circ$ grid resolution using both
 237 statistical methods for all three regions. This regression analysis suggests that the albedo fitted by the
 238 new statistical approach (nonlinear fit) agrees well with the model-simulated albedo over both land
 239 and ocean. The scatter of the results from the nonlinear fit around the 1:1 line is much smaller compared
 240 to multilinear fit, which is also reflected in the coefficients of determination (R^2) ranging from 0.74 to
 241 0.79. However, a reduction in over and underestimation at very large and very small albedos,
 242 respectively, is found in the nonlinear fit compared to the multilinear statistical approach. This is also
 243 clearly reflected in the values for the root mean square error (RMSE), which reduces from 0.042-0.065
 244 to 0.010-0.017, supporting the expectation that the new statistical method is more reliable.
 245 Additionally, a comparison between the planetary albedo computed using both statistical fits and the
 246 CERES retrieved albedo is shown in [Fig. S3S1](#) for all three regions. Similar to the results discussed
 247 above, the analysis shows a good agreement between the CERES derived albedo and the one calculated
 248 using the nonlinear fit.

249 In addition, we performed a comparison of RF_{aci} obtained from satellite measurements using both
 250 statistical approaches with the one simulated by SBDART for each season and for each region. [Fig.](#)
 251 [23](#) illustrates the linear regression of RF_{aci} from the two statistical approaches plotted against the one
 252 obtained from the radiative transfer model for both anthropogenic and natural aerosols for all seasons

253 and all three regions. The analysis showed ~~satisfactory results~~ good statistical agreement with Pearson's
254 correlation coefficient $r=0.82$ and 0.75 and $RMSE=0.037 \text{ Wm}^{-2}$ and 0.042 Wm^{-2} for the anthropogenic
255 and natural fraction of aerosols, respectively. An examination of **Fig. 23** reveals that the nonlinear
256 fitting approach reduces the scatter seen for the multilinear fit and the improvement in correlation with
257 the simulated forcing. ~~Using the~~ The nonlinear fit increases the correlation coefficient by 21%-23%
258 and ~~decreases~~ reduce the RMSE by ~~from~~ 0.007 Wm^{-2} ~~to~~ 0.011 Wm^{-2} compared to the multilinear
259 approach. The relative difference between the RT-simulated and the statistically computed RF_{aci} are
260 computed for both the statistical methods. The mean relative difference in RF_{aci} for anthropogenic
261 fraction of AOD is 0.021 W m^{-2} in the nonlinear and 0.033 W m^{-2} in the multilinear statistical approach,
262 whereas, for RF_{aci} of natural fraction of AOD, it is 0.032 W m^{-2} in nonlinear and 0.053 W m^{-2} in
263 multilinear statistical approach. This suggests that the use of the nonlinear fitting approach reduces the
264 uncertainty by 36%-39% compared to the multilinear regression.

265 4.2 RF_{aci} and Uncertainties

266 ~~Aerosol~~ Aerosols and clouds vary substantially as a function of time in all regions; thus, it is
267 interesting to ~~analyze~~ analyses aerosol-cloud interactions as a function of season. **Fig. 34** shows the
268 seasonal variability of six-year averaged radiative forcing by aerosol-cloud interaction for the three
269 regions as defined above. The maximum anthropogenic RF_{aci} is found over oceanic regions (AS: $-$
270 0.15 Wm^{-2} , BOB: -0.16 Wm^{-2}), instead of regions over land (CI: -0.12 Wm^{-2}) with high anthropogenic
271 emissions. This is because maritime clouds are more susceptible to changes in concentration of
272 anthropogenic aerosols (*Quaas et al., 2008*). In contrast, the natural RF_{aci} is generally stronger over
273 land (-0.15 Wm^{-2}) than over oceanic regions (AS: -0.098 Wm^{-2} , BOB: -0.07 Wm^{-2}). It is seen that the
274 anthropogenic RF_{aci} is strongest during winter over AS and BOB, with values near -0.19 Wm^{-2} and $-$
275 0.22 Wm^{-2} , whereas it is strong (-0.2 Wm^{-2}) during pre-monsoon over CI (land). The dominance of
276 natural aerosols in pre-monsoon results a large natural RF_{aci} both over land (-0.15 Wm^{-2}) and ocean ($-$
277 0.098 Wm^{-2} and -0.07 Wm^{-2}).

278 ~~A~~ A direct comparison of the satellite to simulations-based RF_{aci} , shows a good correlation.
279 However, both satellite estimated and simulated RF_{aci} are subject to errors and it is useful to compute
280 the associated uncertainties in the above results due to various parameters. Uncertainty involves the
281 ones due to satellite retrievals of AOD which can be highly biased in the vicinity of cloud due to
282 swelling (*Koren et al., 2007*), and also due to 3D effects (*Wen et al., 2007*). Since both biases may be
283 particularly high for thick clouds, our estimate of the RF_{aci} could be still be overestimated. The
284 uncertainty in MODIS retrievals of AOD from validation studies (*Levy et al., 2007*) was quantified at
285 $0.03+0.05\tau_a$ over ocean and $0.05+0.15\tau_a$ over land. However, since we use the MODIS-OMI algorithm
286 (*Kim et al., 2007*) to estimate the anthropogenic and natural fraction of AOD, uncertainty in this is
287 given as 1σ standard deviations as per [Table_S2](#). From satellite intercomparison, the uncertainty in
288 radiative flux retrievals by CERES is estimated at 5% (*Loeb, 2004*), and uncertainty in cloud optical
289 depth is 21% (*Minnis et al., 2004*). ~~The computed RF_{aci} in this study is closely~~ The uncertainties due to
290 sensitivity of N_d to a relative change in AOD ($d \ln N_d / d \ln \tau_a$) contribute most to the total uncertainty.
291 For N_d sensitivities to changes in AOD, standard deviations are derived from minimum and maximum
292 values obtained for each season. Following the study by *Bellouin et al., (2013)*, the standard deviations
293 are derived from minimum and maximum values by defining 4-sigma interval, which covers the large
294 range of sensitivities and spatio-temporal variabilities. To define the standard deviations in RF_{aci} due
295 to variation in $d \ln N_d / d \ln \tau_a$, RF_{aci} is recomputed using those standard deviations of N_d sensitivities
296 to changes in AOD. Table 2 shows the seasonal and regional sensitivities of $d \ln N_d / d \ln \tau_a$ along with
297 their statistical standard deviation, which is computed from the minimum and maximum values for

each season. The associated range in RF_{aci} both for anthropogenic and natural fraction of AOD is also shown in Table 2, where the standard deviation of RF_{aci} shows the variation due to change in $d \ln N_d / d \ln \tau_a$, which finally contribute to the total uncertainty. In addition to this, the computed RF_{aci} in this study is associated with the statistical fitting approach as described in section 3. As mentioned earlier, two different statistical fitting methods are used to obtain the regression coefficients for the estimates of RF_{aci} . The study showed that the new nonlinear fitting approach reduces by ~20%–25% the uncertainty from the statistical relationship and fitting parameters. The propagation of error estimate of RF_{aci} . In the present study, except for the statistical fitting method, all the variables and methodologies are same for both the statistical approach. Therefore, we used the relative difference between the RT-simulated and statistically computed RF_{aci} as an uncertainty due to the choice of the statistical fitting approach for both the statistical fitting methods. As shown in section 4.1, the mean relative differences for the nonlinear and multilinear approaches are 0.021 W m^{-2} and 0.033 W m^{-2} , respectively, in RF_{aci} for anthropogenic fraction, whereas, for the RF_{aci} of the natural fraction of AOD, these are 0.032 W m^{-2} and 0.053 W m^{-2} for nonlinear multilinear statistical approaches, respectively. Table 3 lists the uncertainty due to different parameters involved in the satellite-based estimate of RF_{aci} . We quantify the relative error as the square root of the sum of the squared relative errors for all individual contributions. This yields an influence of these relative uncertainties in the input quantities on the computed RF_{aci} of $\sim \pm 0.08 \text{ W m}^{-2}$. It should be noted that we refer here to the published quantifiable uncertainties in the satellite retrievals. Limitation involves involved in this approach or uncertainties in the satellite measurements retrievals contribute to the overall uncertainty but cannot be quantified, which is difficult to quantify.

1—Conclusion

In addition to above error budget, there are uncertainties involved in the RT simulated RF_{aci} due to various parameters as shown above. In this regard, the surface albedo plays a major role in the simulation of RF_{aci} . In the standard approach, we have considered a surface albedo value 0.15 for land and the predefined option for the ocean surface albedo is used for the oceanic regions in the present study. To quantify the uncertainties involved due to assumptions about the surface albedo, we have simulated RF_{aci} with different plausible surface albedo values and computed statistics as shown in Table S3(a) and S3(b). The statistics shows that the considered values of surface albedo are suitably representative of the study regions. In addition, RT simulation have their own limitations and uncertainties e.g. inherent code accuracy, overestimate in calculated RF due to plane-parallel bias, 3-D radiative transfer effect etc. It would be useful to explore these issues in the future. However, in the present study, RT simulation is used to evaluate the results computed with satellite-based measurements. There is a scope to improve the present study with the upcoming data set retrieved from spaceborne active remote sensing instruments, with the improved satellite products and with the new statistical relationship.

5 Conclusions

In this study, we employed a new nonlinear statistical fitting approach to develop the statistical relationship. A satellite-based algorithm is used to quantify the anthropogenic and natural fraction of aerosol optical depth for the computation of RF_{aci} from satellite retrievals. In order to verify, α and RF_{aci} estimates using the new statistical approach (nonlinear) along with the previous statistical approach (multilinear fit), these are compared with the results obtained from radiative transfer simulations. The results show a better agreement between model-based estimates and the one estimated using the nonlinear approach compared to the multilinear approach. The nonlinear approach relatively increases by 21%–23% the correlation coefficient and decreases/reduce RMSE by 0.007 W m^{-2} to 0.011

343 Wm^{-2} ~~the RMSE~~ compared to multilinear approach. The nonlinear fitting approach reduces the relative
344 difference by 36%-39% compare to the multilinear regression method. The RF_{aci} is found to be
345 consistent with the value found by statistical relationship between aerosol and cloud properties from
346 MODIS and CERES, respectively, and radiative transfer calculations. Further studies using the data
347 retrieved from ~~active remote sensing advanced~~ instruments (~~e.g. lidar and radar~~) may be useful to test
348 the assumption made in the present study concerning the proxy of aerosol column, the overestimation
349 of AOD over land and deal with the multi-layer clouds.

350

351 Acknowledgments

352 The authors gratefully acknowledge the constant encouragement received from the Director, SAC for
353 carrying out the present research work. Valuable suggestions received from Deputy Director, EPSA,
354 and Head, CVD also gratefully acknowledged. CERES SSF data were obtained from the NASA
355 Langley Research ~~Center~~Centre Atmospheric Sciences Data ~~Center~~Centre (ASDC), and MODIS data
356 used in this study were acquired as part of NASA(tm)s Earth Science Enterprise. The MODIS Science
357 Teams developed the algorithms for the AOD retrievals. The data were processed by the MODIS
358 Adaptive Processing System for the AOD retrievals. The data were processed by the MODIS Adaptive
359 Processing System and the Goddard Distributed Active Archive (DAAC). The Dutch-Finnish built
360 OMI instrument is part of the NASA EOS Aura satellite payload. The OMI project is managed by
361 NIVR and KNMI in Netherlands. The OMI data were also obtained from the DAAC. Reanalysis data
362 are from the European Centre for Medium-Range Weather Forecasts. The authors would like to thank
363 the data distribution centers for their support, Markand Oza for helpful discussion, and ~~their~~
364 ~~the~~their continuous motivation. JQ acknowledges funding by the European Research Council (GA no
365 306284). The authors are grateful to two anonymous reviewers for constructive and useful comments.

366

367 References

- 368 Albrecht, B. A. (1989). Aerosols, cloud microphysics, and fractional cloudiness. *Science*, 245(4923),
369 1227–1230. doi:10.1126/science.245.4923.1227
- 370 Bellouin, N., Jones, A., Haywood, J., & Christopher, S. A. (2008). Updated estimate of aerosol direct
371 Radiative forcing from satellite observations and comparison against the centre climate model.
372 ~~Journal of Geophysical Research Atmospheres~~, *J. Geophys. Res. Atmos.*, 113(10).
373 doi:10.1029/2007JD009385
- 374 Bellouin, N., Quaas, J., Morcrette, J. J., & Boucher, O. (2013). Estimates of aerosol radiative forcing
375 from the MACC re-analysis. ~~Atmospheric Chemistry and Physics~~, *Atmos. Chem. Phys.*, 13(4),
376 2045–2062. doi:10.5194/acp-13-2045-2013
- 377 Bennartz, R. (2007) Global assessment of marine boundary layer cloud droplet number concentration
378 from satellite. *J. Geophys. Res.*, 112, 10.1029/2006jd007547.
- 379 Bennartz, R., and Rausch, J. (2017) “Global and regional estimates of warm cloud droplet number
380 concentration based on 13 years of AQUA-MODIS observations. *Atmos. Chem. Phys. Discuss.*,
381 doi:10.5194/acp-2016-1130.
- 382 Brenguier, J.-L., Pawlowska, H., Schüller, L., Preusker, R., Fischer, J., & Fouquart, Y. (2000).
383 Radiative Properties of Boundary Layer Clouds: Droplet Effective Radius versus Number
384 Concentration. ~~Journal of the Atmospheric Sciences~~, *J. Atmos. Sci.*, 57(6), 803–821.
- 385 Boucher, O., Randall, D., Artaxo, P., Bretherton, C., Feingold, G., Forster, P., et al. (2013) Clouds and
386 aerosols. In: Stocker TF, Qin D, Plattner GK, Tignor M, Allen SK, Boschung J, et al., editors.
387 Climate change 2013: the physical science basis. Contribution of Working Group I to the Fifth

388 Assessment Report of the Intergovernmental Panel on Climate Change. Cambridge, UK, and New
389 York, NY, USA: Cambridge University Press; pp. 571 – 658.

390 Cherian, R., Venkataraman, C., Quaas, J., Ramachandran, S. (2013). GCM simulations of anthropogenic
391 aerosol-induced changes in aerosol extinction, atmospheric heating and precipitation over India.
392 *Journal of Geophysical Research Atmospheres*, *J. Geophys. Res. Atmos.*, 11:2938–2955.
393 doi:10.1002/jgrd.50298

394 Chin, M., Rood, R.B., Lin, S.J., Muller, J.F., Thompson, A.M., 2000. Atmospheric sulfur cycle
395 simulated in the global model GOCART: model description and global properties. *J. Geophys. Res.*
396 105, 24,671-24,687.

397 Das, S., Dey, S., and Dash, S. K. (2015). Direct radiative effects of anthropogenic aerosols on Indian
398 summer monsoon circulation. *Theoretical and Applied Climatology*, *Theor. Appl. Climatol.*, doi:
399 10.1007/s00704-015-1444-8

400 Feingold, G., Remer, L. A., Ramaprasad, J., and Kaufman, Y. J. (2001). Analysis of smoke impact on
401 clouds in Brazilian biomass burning regions: An extension of Twomey's approach. *Journal of*
402 *Geophysical Research*, *J. Geophys. Res.*, 106, 22907–22922.

403 Feingold, G., Eberhard, W. L., Veron, D. E., and Previdi, M. (2003). First measurements of the
404 Twomey indirect effect using ground-based remote sensors, *Geophysical Research*
405 *Letters*, *Geophys. Res. Lett.*, 30, 1287, doi:10.1029/2002GL016633.

406 Girolamo, L.D., Bond, T.C., Bramer, D., Diner, D.J., Fettingner, F., Kahn, R.A., Martonchik, J.V.,
407 Ramana, M.V., Ramanathan, V., Rasch, P.J., 2004. Analysis of Multi-angle Imaging
408 Spectroradiometer (MISR) aerosol optical depths over greater India during winter 2001 e 2004.
409 *Geophys. Res. Lett.*, 31, L23115. <http://dx.doi.org/10.1029/2004GL021273>.

410 Huber, M., & Knutti, R. (2011). Anthropogenic and natural warming inferred from changes in
411 Earth's energy balance. *Nature Geoscience*, *Nat. Geosci.*, doi:10.1038/ngeo1327

412 Intergovernmental Panel on Climate Change (IPCC) (2007), Climate Change 2007: The Physical
413 Scientific Basis, edited by S. Solomon et al., Cambridge Univ. Press, New York.

414 Kim, J., Lee, J., Lee, H. C., Higurashi, A., Takemura, T., & Song, C. H. (2007). Consistency of the
415 aerosol type classification from satellite remote sensing during the Atmospheric Brown Cloud-East
416 Asia Regional Experiment campaign. *Journal of Geophysical Research Atmospheres*, *J. Geophys.*
417 *Res. Atmos.*, 112(22). doi:10.1029/2006JD008201

418 Koren, I., Remer, L. A., Kaufman, Y. J., Rudich, Y., & Martins, J. V. (2007). On the twilight zone
419 between clouds and aerosols. *Geophysical Research Letters*, *Geophys. Res. Lett.*, 34(8).
420 doi:10.1029/2007GL029253

421 Levelt, P. F., Van Den Oord, G. H. J., Dobber, M. R., Mälkki, A., Visser, H., De Vries, J., ... Saari,
422 H. (2006). The ozone monitoring instrument. *IEEE Transactions on Geoscience and Trans. Geosci.*
423 *Remote Sensing*, *Sens.*, 44(5), 1093–1100. doi:10.1109/TGRS.2006.872333

424 Levenberg, K. (1944). A Method for the Solution of Certain Non-Linear Problems in Least Squares,
425 *Q. Appl. Math.*, 2,164-168.

426 Levy, R. C., Remer, L. A., Mattoo, S., Vermote, E. F., & Kaufman, Y. J. (2007). Second-generation
427 operational algorithm: Retrieval of aerosol properties over land from inversion of Moderate
428 Resolution Imaging Spectroradiometer spectral reflectance. *Journal of Geophysical Research*
429 *Atmospheres*, *J. Geophys. Res. Atmos.*, 112(13). doi:10.1029/2006JD007811

430 Liu, J., Mauzerall, D.L., Horowitz, L.W., 2009. Evaluating inter-continental transport of fine aerosols:
431 (2) global health impact. *Atmos. Environ.* 43, 4339-4347.

432 Loeb, N.: Angular models: Instantaneous and ensemble accuracy, in: 1st CERES-II Science Team
433 Meeting Proceedings, NCAR, Boulder, Colorado, USA, 2004.

434 Loeb, N. G., B. A. Wielicki, W. Su, K. Loukachine, W. Sun, T. Wong, K. J. Priestley, G. Matthews,
435 W. F. Miller, and R. Davies (2007), Multi-instrument comparison of top-of-atmosphere reflected
436 solar radiation, *J. Clim.*, 20, 575–591.

437 Ma, X., Fangqun, Yu., and Quaas, J., (2014). Reassessment of satellite-based estimate of aerosol cloud

438 [forcing. *J. Geophys. Res. Atmos.*, 119, 10,394-10,409, doi:10.1002/2014JD021670.](#)

439 McComiskey, A., Feingold, G., Frisch, A. S., Turner, D. D., Miller, M. A., Chiu, J. C., Min, Q., and

440 Ogren, J. A. (2009). An assessment of aerosol-cloud interactions in marine stratus clouds based on

441 surface remote sensing. ~~*Journal of Geophysical Research*~~, *J. Geophys. Res.*, 114, D09203,

442 doi:10.1029/2008JD011006.

443 McComiskey, A., Feingold, G. (2012). The scale problem in quantifying aerosol indirect effects.

444 ~~*Atmospheric Chemistry and Physics*~~, *Atmos. Chem. Phys.*, 12(2), 1031–1049.

445 Minnis, P., D. F. Young, S. Sun-Mack, P. W. Heck, D. R. Doelling, and Q. Z. Trepte (2003), CERES

446 cloud property retrievals from imagers on TRMM, Terra, and Aqua, in Proc. SPIE 10th International

447 Symposium on Remote Sensing: Conference on Remote Sensing of Clouds and the Atmosphere

448 VII, vol. 5235, pp. 37–48, Barcelona, Spain.

449 Minnis, P., D. F. Young, S. Sun-Mack, Q. Trepte, D. R. Doelling, D. A. Spangenberg, and P. W. Heck

450 (2004), Ceres cloud products, in 1st CERES-II Science Team Meeting Proceedings, NCAR,

451 Boulder, Colorado.

452 Moorthy, K.K., [Babu, S.S., Manoj, M.R., Satheesh, S.K., 2013. Buildup of aerosols over the Indian](#)

453 [region. *Geophys. Res. Lett.* 40, 1011-1014. <http://dx.doi.org/10.1029/2012GL054876>.](#)

454 [Moorthy, K.K.,](#) et al. (2015). South Asian aerosols in perspective: Preface to the special issue.

455 ~~*Atmospheric Environment*~~, *Atmos. Environ.*, <http://dx.doi.org/10.1016/j.atmosenv.2015.10.073>.

456 Parkinson, C. L. (2003). Aqua: An earth-observing satellite mission to examine water and other climate

457 variables. ~~*IEEE Transactions on Geoscience and Trans.*~~ *Geosci. Remote Sensing, Sens.*, 41, 173–

458 183. doi:10.1109/TGRS.2002.808319

459 Penner, J. E., Xu, L., & Wang, M. (2011). Satellite methods underestimate indirect climate forcing by

460 aerosols. ~~*Proceedings of the National Academy of Sciences of the United States of America*~~, *Proc.*

461 [Natl. Acad. Sci. U.S.A.](#), 108(33), 13404–13408. doi:10.1073/pnas.1018526108

462 Penner, J. E., Zhou, C., & Xu, L. (2012). Consistent estimates from satellites and models for the first

463 aerosol indirect forcing. ~~*Geophysical Research Letters*~~, *Geophys. Res. Lett.*, 39(13).

464 doi:10.1029/2012GL051870

465 Quaas, J., Boucher, O., Bellouin, N., & Kinne, S. (2008). Satellite-based estimate of the direct and

466 indirect aerosol climate forcing. ~~*Journal of Geophysical Research: Atmospheres*~~, *J. Geophys. Res.*

467 [Atmos.](#), 113(5), 1–9. doi:10.1029/2007JD008962

468 Quaas, J., Boucher, O., & Bréon, F. M. (2004). Aerosol indirect effects in POLDER satellite data and

469 the Laboratoire de Météorologie Dynamique-Zoom (LMDZ) general circulation model. ~~*Journal of*~~

470 ~~*Geophysical Research D: Atmospheres*~~, *J. Geophys. Res. Atmos.*, 109(8).

471 doi:10.1029/2003JD004317

472 [Quaas, J., O. Boucher, and U. Lohmann \(2006\), Constraining the total aerosol indirect effect in the](#)

473 [LMDZ and ECHAM4 GCMs using MODIS satellite data, *Atmos. Chem. Phys.*, 6, 947–955.](#)

474 Quaas, J., Ming, Y., Menon, S., Takemura, T., Wang, M., Penner, J. E., ... Schulz, M. (2009). Aerosol

475 indirect effects – general circulation model intercomparison and evaluation with satellite data.

476 ~~*Atmospheric Chemistry and Physics*~~, *Atmos. Chem. Phys.*, 9(22), 8697–8717. doi:10.5194/acp-9-

477 8697-2009

478 Quaas, J., O. Boucher, N. Bellouin, and S. Kinne (2011), Which of satellite- or model-based estimates

479 is closer to reality for aerosol indirect forcing?, *Proc. Natl. Acad. Sci. U.S.A.*, 108, E1099.

480 [Rausch, J., Heidinger, A., and Bennartz, R. \(2010\). Regional assessment of microphysical properties](#)

481 [of marine boundary layer cloud using the PATMOS-x dataset, *J. Geophys. Res. Atmos.*, 115,](#)

482 [10.1029/2010jd014468.](#)

483 Remer, L. A., Kaufman, Y. J., Tanré, D., Mattoo, S., Chu, D. A., Martins, J. V., ... Holben, B. N.

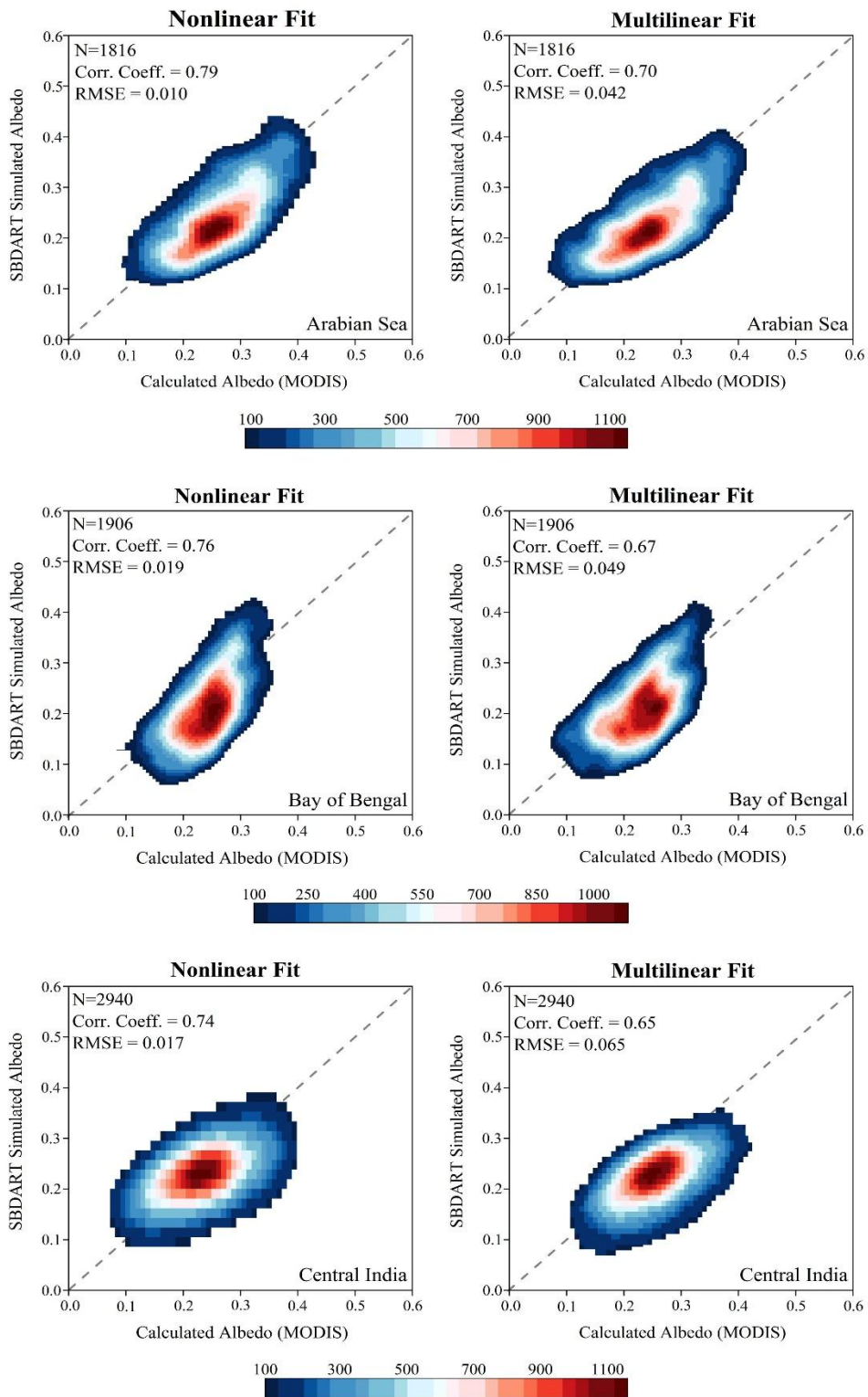
484 (2005). The MODIS Aerosol Algorithm, Products, and Validation. ~~*Journal of the Atmospheric*~~

485 ~~*Sciences*~~, *J. Atmos. Sci.*, 62(4), 947–973. doi:10.1175/JAS3385.1

486 Ricchiazzi, P., Yang, S., Gautier, C., & Sowle, D. (1998). SBDART: A Research and Teaching

487 Software Tool for Plane-Parallel Radiative Transfer in the Earth's Atmosphere. ~~*Bulletin of the*~~

488 *American Meteorological Society, B. Am. Meteorol. Soc.*, 79(10), 2101–2114.
489 Schoeberl, M. R., Douglass, A. R., Hilsenrath, E., Bhartia, P. K., Beer, R., Waters, J. W., ... DeCola,
490 P. (2006). Overview of the EOS aura mission. IEEE *Transactions on Geoscience and Trans. Geosci.*
491 *Remote Sensing, Sens.*, 44(5), 1066–1072. doi: 10.1109/TGRS.2005.861950
492 Schüller, L., R. Bennartz, J. Fischer, and J.-L. Brenguier (2005), An algorithm for the retrieval of
493 droplet number concentration and geometrical thickness of stratiform marine boundary layer clouds
494 applied to MODIS radiometric observations, *J. Appl. Meteorol.*, 44, 28– 38.
495 Stamnes, K., Tsay, S. C., Wiscombe, W., & Jayaweera, K. (1988). Numerically stable algorithm for
496 discrete-ordinate-method radiative transfer in multiple scattering and emitting layered media.
497 *Applied Optics*, 27(12), 2502–2509. doi:10.1364/AO.27.002502
498 Tiwari, S., Mishra, A. K., and Singh, A K. (2015). Aerosol climatology over the Bay of Bengal and
499 Arabian Sea inferred from space-borne radiometers and lidar observations. *Aerosol and Air Quality*
500 *Research, Qual. Res.*, doi:10.4209/aaqr.2015.06.0406.
501 Torres, O., Bhartia, P. K., Herman, J. R., Ahmad, Z., & Gleason, J. (1998). Derivation of aerosol
502 properties from satellite measurements of backscattered ultraviolet radiation: Theoretical basis.
503 *Journal of Geophysical Research: Atmospheres, J. Geophys. Res. Atmos.*, 103(D14), 17099–17110.
504 doi: 10.1029/98JD00900
505 Transtrum, M. K., Machta, B. B., and Sethna, J.P. (2010). Why are nonlinear fits to data so
506 challenging? *Phys. Rev. Lett.* 104, 060201.
507 Transtrum, M. K., and Sethna, J.P. (2012). Improvements to the Levenberg-Marquardt algorithm for
508 nonlinear least-squares minimization. *J. Comput. Phys.*, <https://arXiv.org/abs/1201.5885v1>.
509 Twomey, S. (1977). The Influence of Pollution on the Shortwave Albedo of Clouds. *Journal of the*
510 *Atmospheric Sciences, J. Atmos. Sci.*
511 Wen, G., Marshak, A., Cahalan, R. F., Remer, L. A., & Kleidman, R. G. (2007). 3-D aerosol-cloud
512 radiative interaction observed in collocated MODIS and ASTER images of cumulus cloud fields.
513 *Journal of Geophysical Research Atmospheres, J. Geophys. Res. Atmos.*, 112(13).
514 doi:10.1029/2006JD008267
515 Wielicki, B. A., Barkstrom, B. R., Harrison, E. F., Lee, R. B., Smith, G. L., & Cooper, J. E. (1996).
516 Clouds and the Earth's Radiant Energy System (CERES): An Earth Observing System Experiment.
517 *Bulletin of the American Meteorological Society, B. Am. Meteorol. Soc.*, 77(5), 853–868.
518
519



522 **Figure 1.**

523 **Table 1:** The list of parameters and their sources used as an input to the SDBART model for the
 524 simulation of RF_{aci} .

<u>Input parameters</u>	<u>Source</u>
<u>Temperature and Water vapor (for 32 layers extending from 1000 to 1 hPa)</u>	<u>ECMWF reanalysis</u>
<u>Total Columnar ozone</u>	<u>OMI-AURA</u>
<u>Surface Albedo</u>	<u>For land - 0.15</u> <u>For ocean - default value of "ocean" (given in SBDART)</u>
<u>cloud effective droplet radius</u> <u>cloud liquid water path</u> <u>cloud fraction</u>	<u>MODIS retrievals reported in CERES-SSF product</u>
<u>geometrical thickness of cloud</u>	<u>Computed from MODIS and ECMWF data</u>

527

528

529

530

531

532

Table 2: Seasonal and regional sensitivities $d \ln N_d / d \ln \tau_a$ of cloud droplet number concentration N_d to changes in aerosol optical depth used in this study. The given standard deviation is derived from minimum and maximum values for a particular season. The associated range in RF_{aci} is also estimated where the standard deviation of RF_{aci} shows the variation due to change in $d \ln N_d / d \ln \tau_a$.

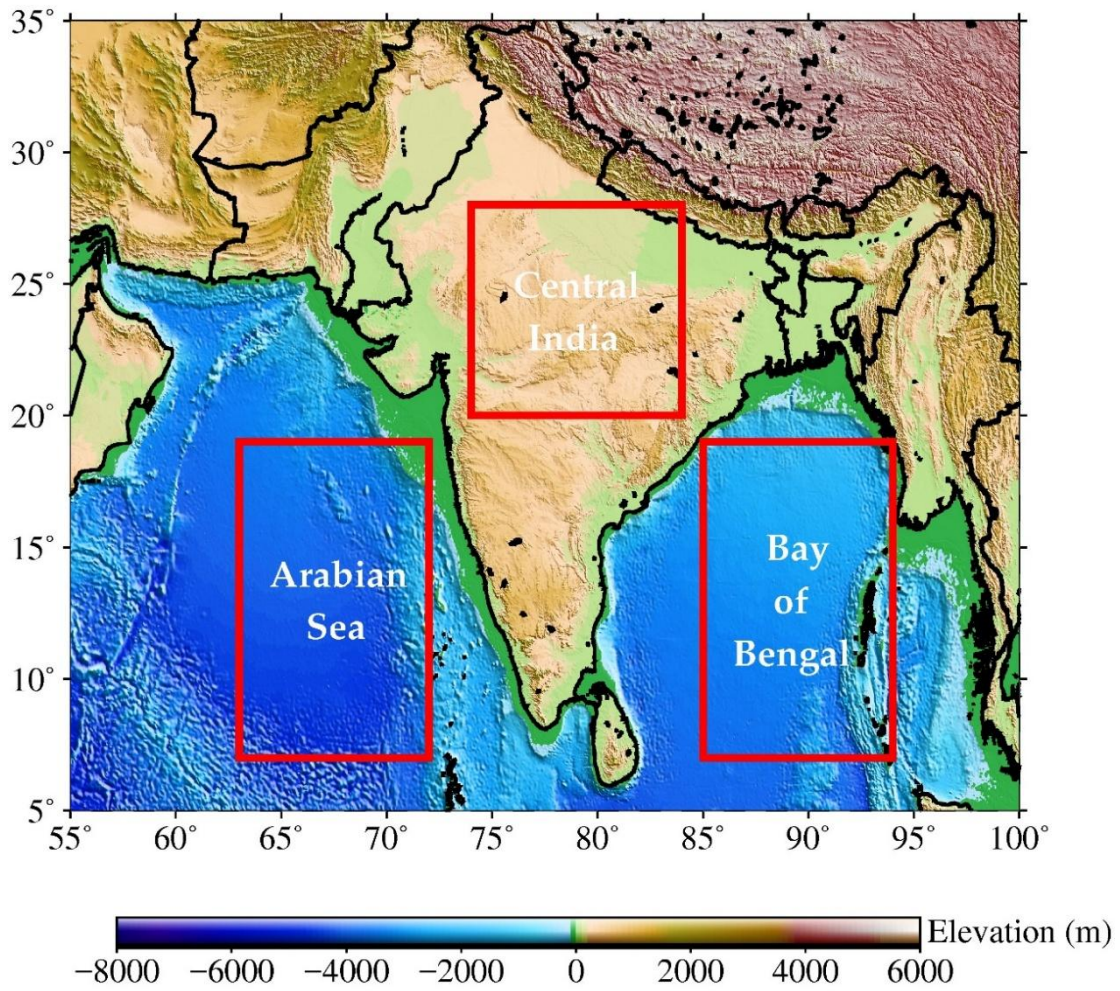
	Region	Winter	Pre-Monsoon	Monsoon	Post-Monsoon ⁵³³
$\frac{d \ln N_d}{d \ln \tau}$	AS	<u>0.384 ± 0.146</u>	<u>0.408 ± 0.189</u>	<u>0.272 ± 0.131</u>	<u>0.18 ± 0.102</u> ⁵³⁴
	BOB	<u>0.314 ± 0.136</u>	<u>0.414 ± 0.15</u>	<u>0.194 ± 0.104</u>	<u>0.148 ± 0.088</u>
	CI	<u>0.214 ± 0.107</u>	<u>0.178 ± 0.105</u>	<u>0.107 ± 0.069</u>	<u>0.122 ± 0.071</u>
RF_{aci} for Anthrophonic Fraction	AS	<u>-0.19 ± 0.036</u>	<u>-0.14 ± 0.056</u>	<u>-0.08 ± 0.036</u>	<u>-0.16 ± 0.036</u>
	BOB	<u>-0.22 ± 0.062</u>	<u>-0.16 ± 0.036</u>	<u>-0.07 ± 0.02</u>	<u>-0.2 ± 0.036</u>
	CI	<u>-0.13 ± 0.02</u>	<u>-0.2 ± 0.036</u>	<u>-0.05 ± 0.034</u>	<u>-0.16 ± 0.036</u>
RF_{aci} for Natural Fraction	AS	<u>-0.12 ± 0.036</u>	<u>-0.18 ± 0.036</u>	<u>-0.03 ± 0.04</u>	<u>-0.06 ± 0.036</u>
	BOB	<u>-0.08 ± 0.026</u>	<u>-0.11 ± 0.026</u>	<u>-0.04 ± 0.039</u>	<u>-0.06 ± 0.017</u>
	CI	<u>-0.16 ± 0.027</u>	<u>-0.22 ± 0.055</u>	<u>-0.1 ± 0.027</u>	<u>-0.14 ± 0.036</u>

535
536
537

Table 3: Lists the sources of uncertainties and their values involved in the satellite-based estimate of RF_{aci} in the present study.

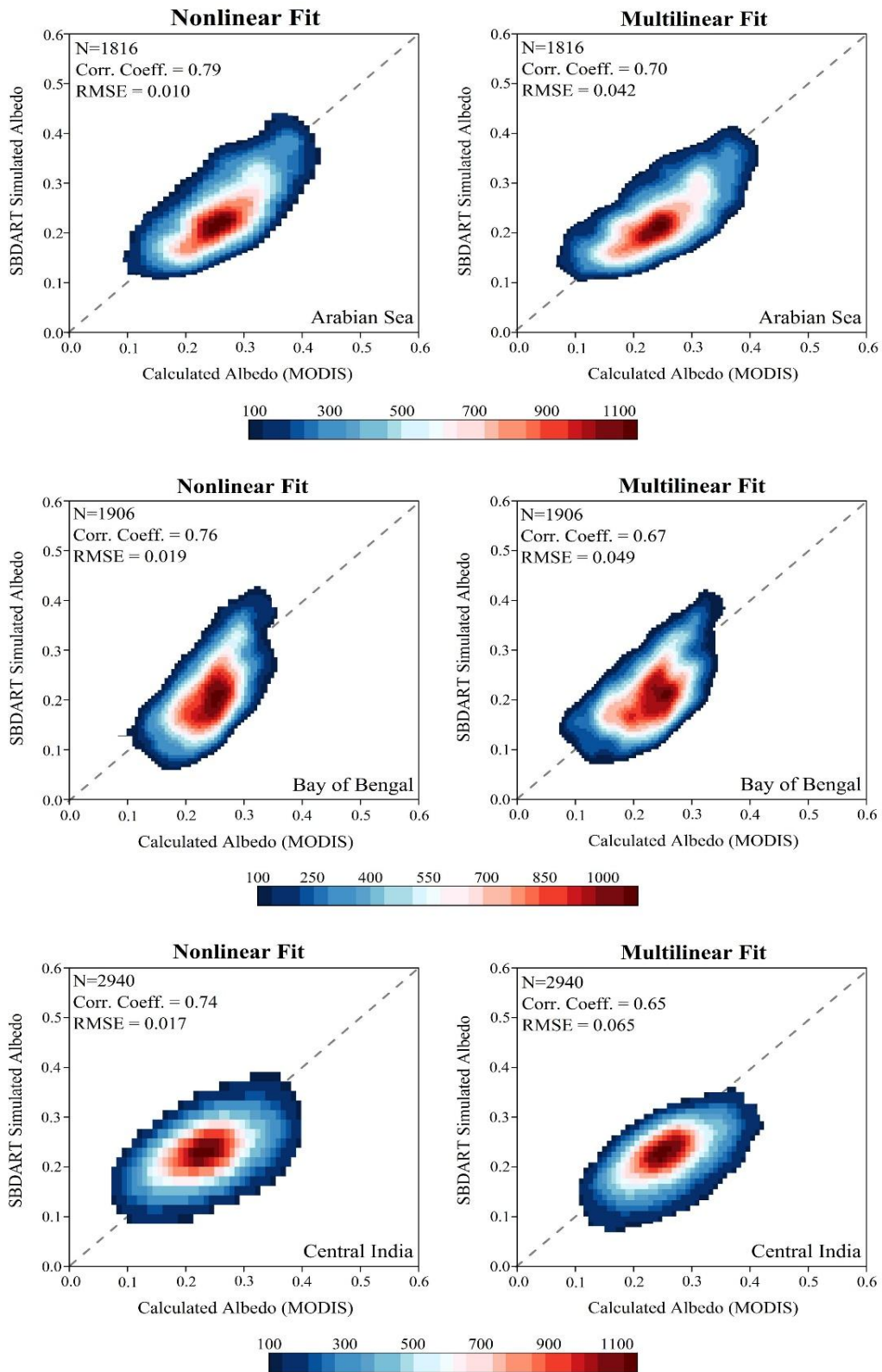
<u>Source of uncertainty</u>	<u>Values</u>	538
		539
		540
<u>Total AOD</u>	<u>$0.03 \pm 0.05 \cdot \tau_a$ over ocean</u> <u>$0.05 \pm 0.05 \cdot \tau_a$ over land</u>	541
<u>MODIS-OMI algorithm</u> <u>(for the estimate of anthropogenic</u> <u>and natural fraction of aerosol)</u>	<u>1σ standard deviation as per</u> <u>below table-S2</u>	
<u>Flux retrieval from CERES</u>	<u>5%</u>	
<u>Cloud optical depth retrieval from</u> <u>CERES</u>	<u>21%</u>	
<u>Cloud droplet number concentration</u>	<u>See table-2</u>	
<u>Statistical fitting approach</u>	<u>0.021 W m^{-2} in nonlinear for anthropogenic</u> <u>0.032 W m^{-2} in nonlinear for natural</u> <u>0.033 W m^{-2} in multilinear for anthropogenic</u> <u>0.053 W m^{-2} in multilinear for natural</u>	

542
543
544



545
546
547
548

Figure 1: Map of India and surroundings showing the study regions. The regions covered by red box represent the study locations (Arabian Sea, Bay of Bengal and Central India).



549

550 **Figure 2:** Scatter density plots of model-simulated albedo and the one computed using both statistical
 551 fitting method (nonlinear and multilinear fit) using satellite measurements for all three regions.

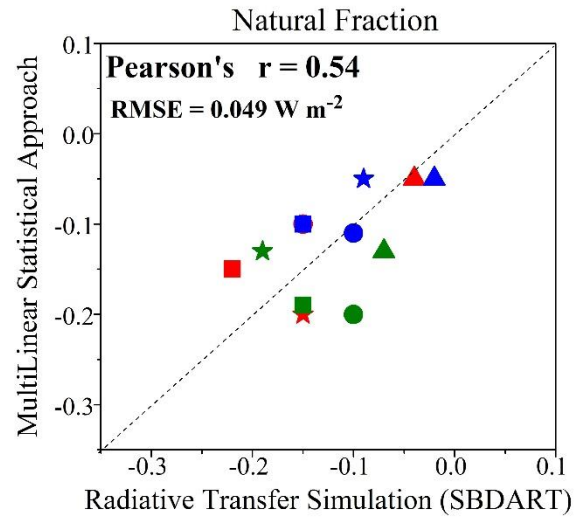
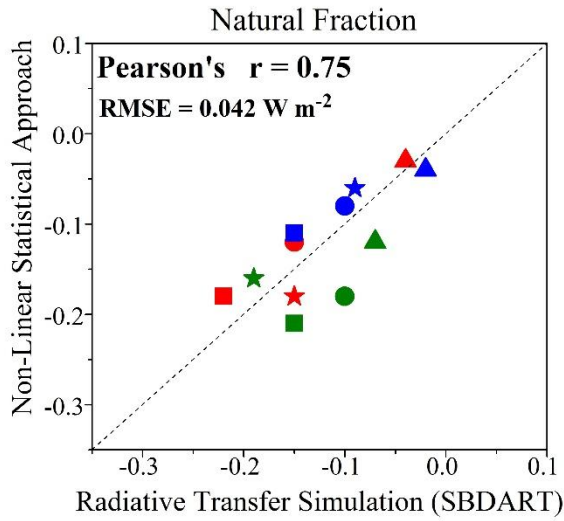
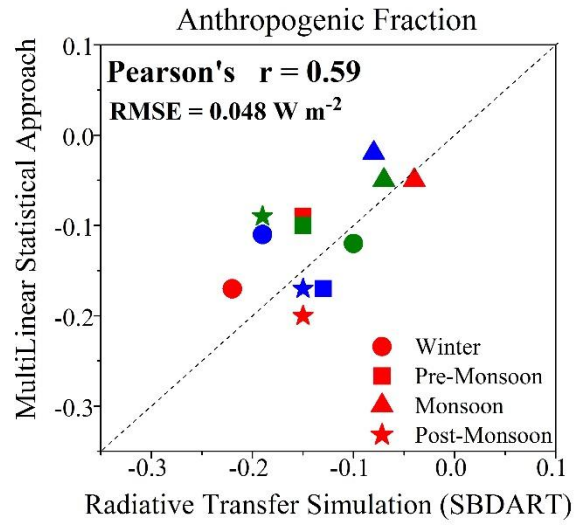
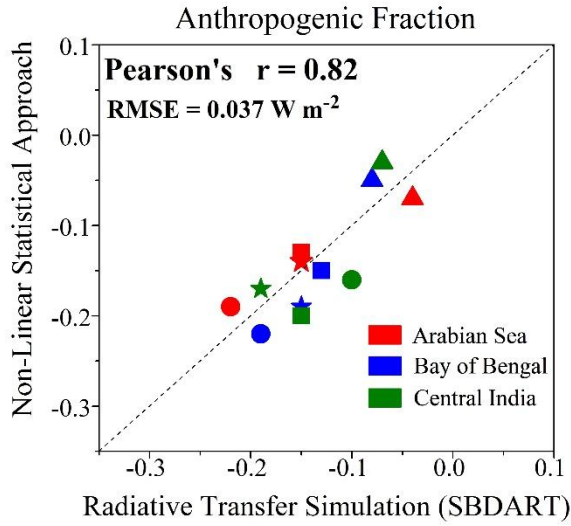
552

553

554

555

First Indirect Radiative Forcing ($W m^{-2}$)

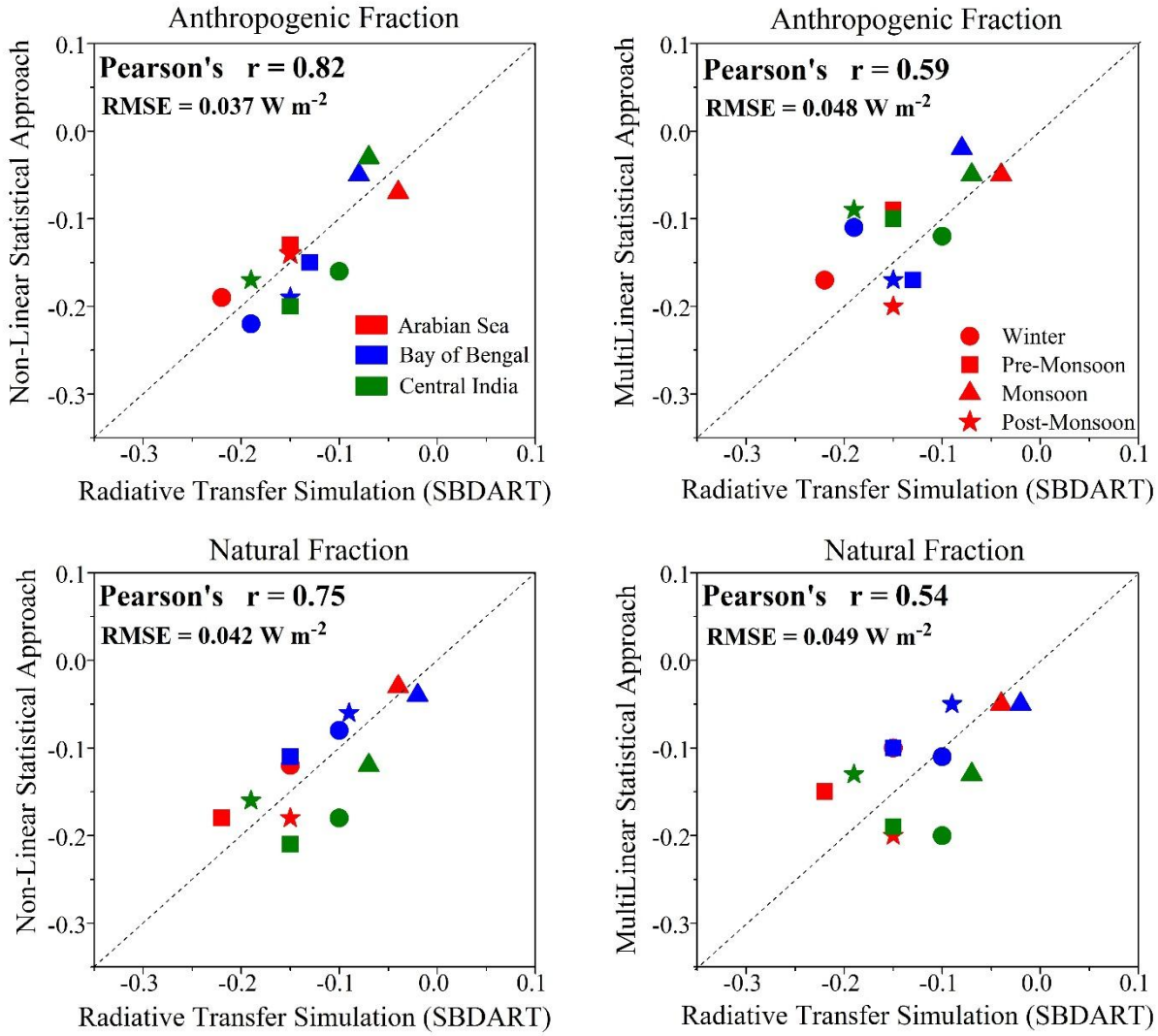


556

557

558
559
560

First Indirect Radiative Forcing (W m^{-2})



561

562 **Figure 3-:** Comparison between satellite-based RFacI using both statistical fits and the one simulated
563 by the SBDART model for all three regions and for all seasons. The different color indicates the
564 regions, whereas the different symbols indicates the different seasons. -Note that the fit is separately
565 performed for each season and each region.

566

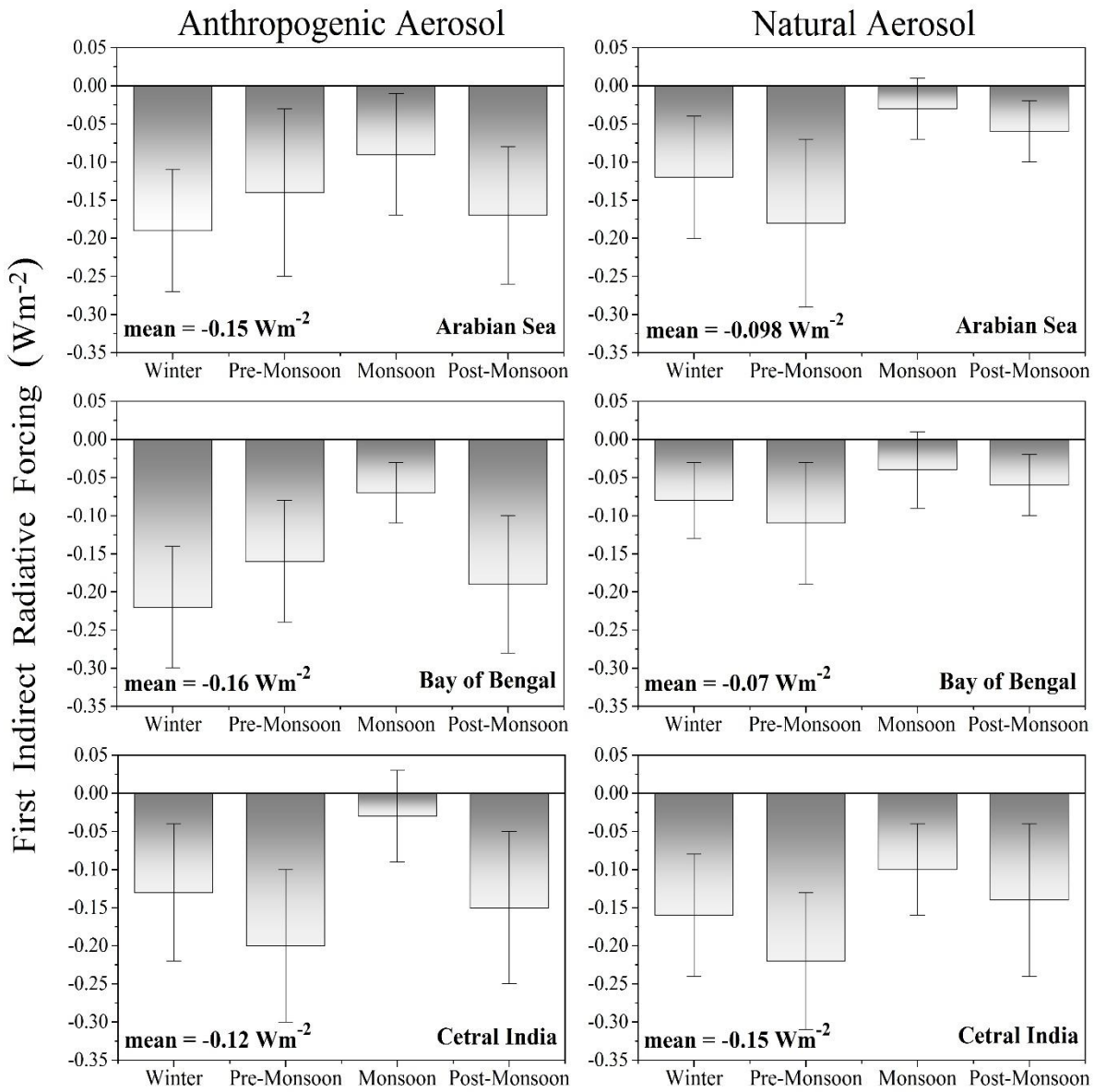
567

568

569

570

571



572

573 **Figure 4:** Seasonal variability of six-year averaged RF_{aci} obtained using the nonlinear fit for all
574 three regions for both anthropogenic and natural aerosols along with mean values.

Table S4.: The seasonal and regional variation of fitting parameters α_1 - α_6 obtained from both multilinear and nonlinear fitting approaches.

Area	Season	Nonlinear fit						Multilinear regression fit					
		α_1	α_2	α_3	α_4	α_5	α_6	α_1	α_2	α_3	α_4	α_5	α_6
Arabian Sea	Winter	0.158	0.023	0.376	0.232	0.199	0.943	0.098	0.101	0.002	0.005	1.000	0.303
	Pre-Monsoon	0.136	0.021	-0.046	0.205	0.201	0.888	0.089	0.067	0.008	0.010	1.000	0.416
	Monsoon	0.109	0.029	-0.046	0.395	0.201	0.888	0.092	0.049	0.009	0.012	1.000	0.422
	Post-Monsoon	0.154	0.026	0.108	0.010	1.192	0.172	0.091	0.097	0.044	0.024	1.000	0.558
Bay of Bengal	Winter	0.158	0.024	-0.084	0.209	0.140	0.652	0.100	0.084	0.345	0.088	1.000	0.136
	Pre-Monsoon	0.127	0.012	-0.043	0.081	0.081	0.474	0.092	0.060	0.004	0.002	1.000	0.324
	Monsoon	0.126	0.011	-0.398	0.415	0.006	0.473	0.095	0.046	0.011	0.005	1.000	0.414
	Post-Monsoon	0.150	0.020	0.331	0.311	0.119	1.097	0.100	0.071	0.014	0.007	1.000	0.364
Central India	Winter	0.215	0.010	-0.278	0.685	0.105	1.236	0.187	0.026	0.079	0.084	1.000	0.269
	Pre-Monsoon	0.183	0.003	-0.259	0.662	0.099	1.339	0.171	0.018	0.020	0.009	1.000	0.278
	Monsoon	0.187	0.007	0.322	0.390	0.098	0.555	0.168	0.024	0.002	0.005	1.000	0.319
	Post-Monsoon	0.210	0.016	-0.291	0.684	0.105	1.444	0.174	0.042	0.000	0.005	1.000	0.253

577

578

579

580 **Table S2:** Mean seasonal variation of anthropogenic and natural fraction of aerosol optical
 581 depth over all three regions estimated using methodology by *Kim et al., (2007)*.

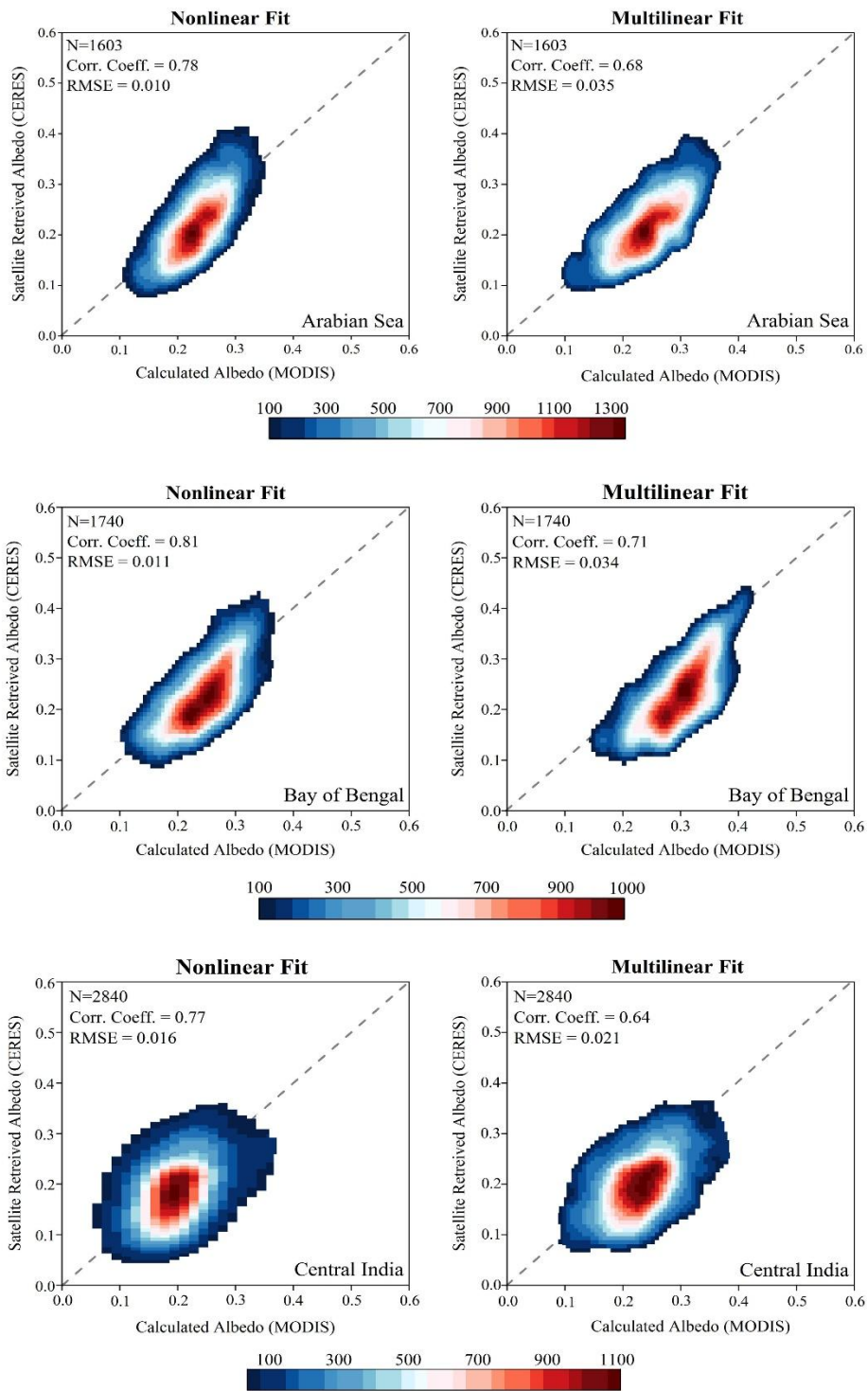
	Arabian Sea (AS)		Bay of Bengal (BOB)		Central India (CI)	
	Anthro*	Nat*	Anthro	Nat	Anthro	Nat
Winter	0.146±0.029	0.112±0.022	0.16±0.032	0.142±0.028	0.376±0.055	0.279±0.056
Pre- Monsoon	0.305±0.061	0.347±0.069	0.309±0.062	0.327±0.065	0.407±0.081	0.46±0.092
Monsoon	0.113±0.023	0.346±0.069	0.16±0.032	0.276±0.055	0.435±0.087	0.655±0.101
Post- Monsoon	0.309±0.062	0.298±0.059	0.305±0.061	0.234±0.046	0.627±0.095	0.505±0.089

582 *Anthro represents anthropogenic and Nat represents natural

583

584

585
586



587

588 **Table S3(a):** The statistics calculated for a different plausible values of surface albedo over land.

589

590

591

<u>Calculated (MODIS) Vs. Simulated (SBDART)</u>	<u>Land type</u>	<u>Land Surface Albedo</u>	<u>Nonlinear fit</u>		<u>Multilinear fit</u>	
			<u>R</u>	<u>RMSE</u>	<u>R</u>	<u>RMSE</u>
<u>Planetary albedo</u>	<u>Present study</u>	<u>0.15</u>	<u>0.74</u>	<u>0.017</u>	<u>0.65</u>	<u>0.065</u>
	<u>Forest</u>	<u>0.14</u>	<u>0.72</u>	<u>0.019</u>	<u>0.63</u>	<u>0.067</u>
	<u>Cropland</u>	<u>0.20</u>	<u>0.69</u>	<u>0.023</u>	<u>0.59</u>	<u>0.071</u>
	<u>Grass land</u>	<u>0.21</u>	<u>0.67</u>	<u>0.025</u>	<u>0.56</u>	<u>0.074</u>
	<u>Barren land</u>	<u>0.38</u>	<u>0.62</u>	<u>0.033</u>	<u>0.50</u>	<u>0.079</u>
<u>First Indirect Forcing by Anthropogenic fraction</u>	<u>Present study</u>	<u>0.15</u>	<u>0.83</u>	<u>0.037</u>	<u>0.62</u>	<u>0.048</u>
	<u>Forest</u>	<u>0.14</u>	<u>0.73</u>	<u>0.039</u>	<u>0.55</u>	<u>0.050</u>
	<u>Cropland</u>	<u>0.20</u>	<u>0.69</u>	<u>0.043</u>	<u>0.50</u>	<u>0.055</u>
	<u>Grass land</u>	<u>0.21</u>	<u>0.66</u>	<u>0.044</u>	<u>0.49</u>	<u>0.057</u>
	<u>Barren land</u>	<u>0.38</u>	<u>0.60</u>	<u>0.050</u>	<u>0.45</u>	<u>0.062</u>
<u>First Indirect Forcing by Natural fraction</u>	<u>Present study</u>	<u>0.15</u>	<u>0.77</u>	<u>0.042</u>	<u>0.54</u>	<u>0.049</u>
	<u>Forest</u>	<u>0.14</u>	<u>0.71</u>	<u>0.043</u>	<u>0.50</u>	<u>0.050</u>
	<u>Cropland</u>	<u>0.20</u>	<u>0.66</u>	<u>0.045</u>	<u>0.48</u>	<u>0.051</u>
	<u>Grass land</u>	<u>0.21</u>	<u>0.62</u>	<u>0.047</u>	<u>0.47</u>	<u>0.053</u>
	<u>Barren land</u>	<u>0.38</u>	<u>0.59</u>	<u>0.052</u>	<u>0.45</u>	<u>0.060</u>

592

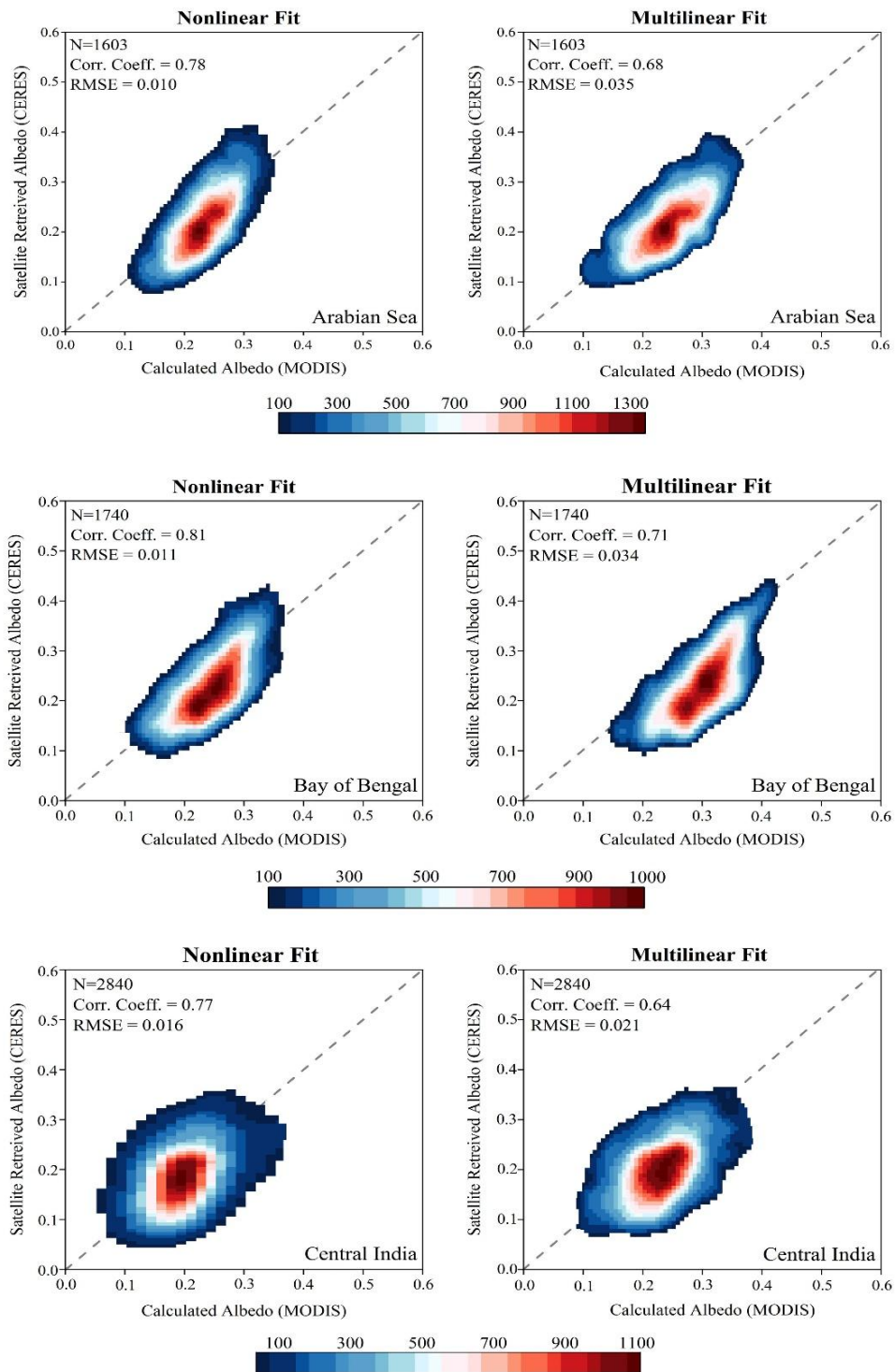
593

594

595 **Table S3(b):** The statistics calculated for the different plausible values of surface albedo over
 596 ocean.

<u>Calculated</u> <u>(MODIS)</u> <u>Vs.</u> <u>Simulated</u> <u>(SBDART)</u>	<u>Ocean</u> <u>Surface</u> <u>Albedo</u>	<u>Nonlinear fit</u>				<u>Multilinear fit</u>			
		<u>R</u>		<u>RMSE</u>		<u>R</u>		<u>RMSE</u>	
		<u>AS</u>	<u>BOB</u>	<u>AS</u>	<u>BOB</u>	<u>AS</u>	<u>BOB</u>	<u>AS</u>	<u>BOB</u>
<u>Planetary</u> <u>albedo</u>	<u>Present</u> <u>study</u>	<u>0.79</u>	<u>0.76</u>	<u>0.010</u>	<u>0.019</u>	<u>0.70</u>	<u>0.67</u>	<u>0.042</u>	<u>0.049</u>
	<u>0.13</u>	<u>0.69</u>	<u>0.67</u>	<u>0.021</u>	<u>0.029</u>	<u>0.61</u>	<u>0.59</u>	<u>0.059</u>	<u>0.059</u>
	<u>0.11</u>	<u>0.75</u>	<u>0.73</u>	<u>0.013</u>	<u>0.022</u>	<u>0.66</u>	<u>0.63</u>	<u>0.047</u>	<u>0.052</u>
	<u>0.08</u>	<u>0.71</u>	<u>0.7</u>	<u>0.017</u>	<u>0.026</u>	<u>0.63</u>	<u>0.61</u>	<u>0.053</u>	<u>0.055</u>
	<u>0.06</u>	<u>0.68</u>	<u>0.65</u>	<u>0.023</u>	<u>0.03</u>	<u>0.59</u>	<u>0.58</u>	<u>0.056</u>	<u>0.061</u>
<u>First Indirect</u> <u>Forcing by</u> <u>Anthropogenic</u> <u>fraction</u>	<u>Present</u> <u>study</u>	<u>0.89</u>	<u>0.87</u>	<u>0.035</u>	<u>0.037</u>	<u>0.68</u>	<u>0.68</u>	<u>0.047</u>	<u>0.048</u>
	<u>0.13</u>	<u>0.83</u>	<u>0.8</u>	<u>0.041</u>	<u>0.043</u>	<u>0.60</u>	<u>0.59</u>	<u>0.060</u>	<u>0.061</u>
	<u>0.11</u>	<u>0.87</u>	<u>0.85</u>	<u>0.037</u>	<u>0.04</u>	<u>0.64</u>	<u>0.64</u>	<u>0.055</u>	<u>0.054</u>
	<u>0.08</u>	<u>0.81</u>	<u>0.83</u>	<u>0.039</u>	<u>0.041</u>	<u>0.60</u>	<u>0.61</u>	<u>0.059</u>	<u>0.057</u>
	<u>0.06</u>	<u>0.78</u>	<u>0.78</u>	<u>0.042</u>	<u>0.045</u>	<u>0.58</u>	<u>0.56</u>	<u>0.065</u>	<u>0.067</u>
<u>First Indirect</u> <u>Forcing by</u> <u>Natural</u> <u>fraction</u>	<u>Present</u> <u>study</u>	<u>0.86</u>	<u>0.85</u>	<u>0.039</u>	<u>0.038</u>	<u>0.61</u>	<u>0.65</u>	<u>0.049</u>	<u>0.051</u>
	<u>0.13</u>	<u>0.74</u>	<u>0.76</u>	<u>0.046</u>	<u>0.047</u>	<u>0.51</u>	<u>0.57</u>	<u>0.055</u>	<u>0.060</u>
	<u>0.11</u>	<u>0.83</u>	<u>0.83</u>	<u>0.040</u>	<u>0.041</u>	<u>0.58</u>	<u>0.62</u>	<u>0.051</u>	<u>0.053</u>
	<u>0.08</u>	<u>0.80</u>	<u>0.79</u>	<u>0.042</u>	<u>0.044</u>	<u>0.54</u>	<u>0.60</u>	<u>0.054</u>	<u>0.057</u>
	<u>0.06</u>	<u>0.72</u>	<u>0.75</u>	<u>0.049</u>	<u>0.051</u>	<u>0.50</u>	<u>0.55</u>	<u>0.058</u>	<u>0.061</u>

597



598

599

Figure S3-S1: Scatter density plots CERES-retrieved α vs. calculated α for all three regions.

600

601